ISSN 0256-4637
VOLUME 42 NUMBER 3 JULY-SEPTEMBER 2020

Journal of Pure and Applied

Ultrasonics

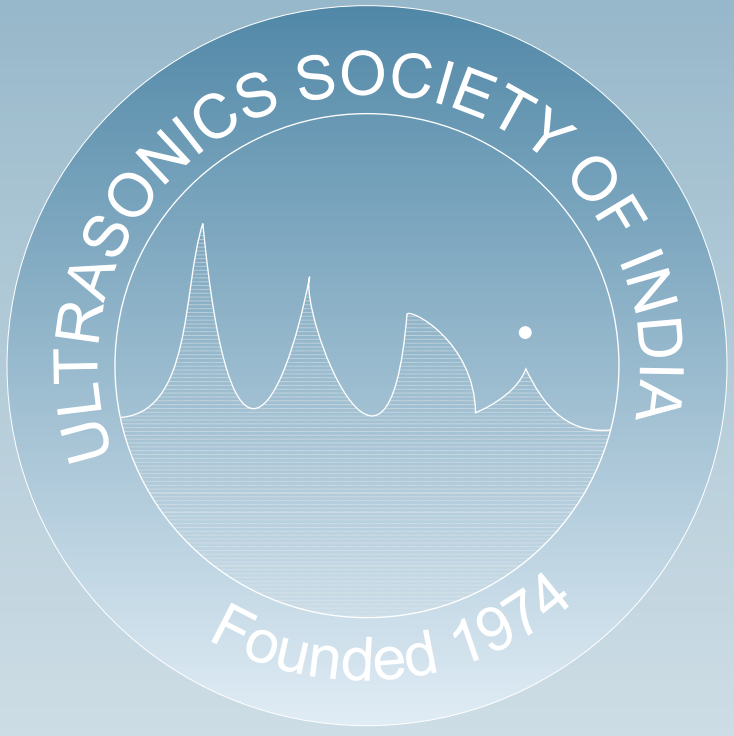

Website : www.ultrasonicsindia.org

A Publication of Ultrasonics Society of India

A Quarterly Publication of Ultrasonics Society of India

Journal of Pure and Applied

Ultrasonics

No. 3	Volume 42	July-September 2020

SUBSCRIPTION (postage paid)

Single	Rs. 750/-	US$ 60/-
Annual	Rs. 3000/-	US$ 250/-
USI *members*	Free	

The submission of papers and all other correspondence regarding the Journal may please be addressed to :

Publication Secretary
Journal of Pure and Applied Ultrasonics
C/o Ultrasonics Society of India
CSIR-National Physical Laboratory
Dr. K.S. Krishnan Road, New Delhi-110012
publicationsecretary.usi@gmail.com
www.ultrasonicsindia.org

ISSN 0256–4637

Journal of Pure and Applied Ultrasonics

VOLUME 42 NUMBER 3 JULY-SEPTEMBER 2020

CONTENTS

Editorial – Some directions for study of thermoelastic properties of solids for future applications 58
Dr. S.K. Jain

Synthesis and spectroscopic characterization of Boehmite nanoparticles and its thermodynamic study 59
N.R. Pawar, Mrunal Pawar, R.D. Chavhan and O.P. Chimankar

Temperature and frequency dependence of acoustic attenuation in pure semiconductors 66
Sanjay H. Bagade

Acoustic and refractive behaviour of the binary mixture of 1-butyl-3methylimidazolium tetrafluoroborate with 1-alkanol at 298.15 to 313.15K 72
Ankit Gupta, V. S. Gangwar, Ashish Kumar Singh, S. K. Singh and R.K. Shukla

Elastic and ultrasonic properties of cadmium oxide 78
Jyoti Bala, Vyoma Bhalla, Devraj Singh, C.P. Yadav and D.K. Pandey

Ph.D. Thesis Summary 81
Study of Ultrasonic and Thermal Properties of Materials for Industrial Applications
Shakti Pratap Singh

(Authors have stated that the papers have not been published elsewhere)

Website : www.ultrasonicsindia.org

A Publication of — Ultrasonics Society of India

EDITORIAL

Some directions for study of thermoelastic properties of solids for future applications

Dear Colleagues,

Since the last issue, one major development has been that Prof. (Dr.) Raja Ram Yadav, who is Vice-President of Ultrasonics Society of India (USI) and Member of Editorial Board of the journal, has completed his tenure of Vice-Chancellor at VBS Purvanchal University, Jaunpur in July 2020 with accolades and is presently Professor of Physics at Allahabad University. The last conference of USI (ICUMSAT-2019) was organized under his guidance at this University at Jaunpur, the highlights of which were reported in last issue.

The present issue of JPAU brings to you more of physical ultrasonics research in some material systems including crystalline solids, nano-particle fluid, liquid mixtures, etc. Computational studies of elastic properties of various solids have been recognized as significant method for brittle materials in particular where it is difficult to measure these properties. With the availability of efficient computational power it has become possible to compute elastic and thermal properties of solids with sufficient precision, which can be used in design of these materials for various applications. Computational elastic constants have been verified on materials amenable for measurements.

JPAU has regularly published papers on theoretical computation of elastic and thermal properties of intermetallic, semiconductor, rare-earth materials for elastic, an-harmonic, anisotropic, Debye temperature, specific heat, thermal expansion constants, etc., using the Born-Mayer potential theory, Debye-grüneisen theory, density function theory and using the lattice parameter values. Authors of such work are encouraged to extend their work from single crystals to estimating the elastic properties of polycrystalline materials using averaging methods reported in literature in recent years. The properties of polycrystalline materials are isotropic, unless the material is stressed, and are significantly different as compared to single crystals, which are normally anisotropic. It would be particularly of significance for thin films for their applications in accelerometers, capacitive multi-array transducers, etc.

Another significant area currently being reported in literature is the work on computational elastic constants to estimate the internal stresses in materials having residual stresses. Residual stresses are generated during cooling of moulds of materials, weld joints, extruded materials, which are widely used in many applications. As internal stresses cannot be measured directly, they can be calculated indirectly from the internal strains measured mechanically in terms of internally produced curvature in materials or X-ray methods. These studies can play a powerful role in assisting non-destructive evaluation of thermally stressed materials, weld joints, extruded parts, etc. by computing the internal stresses. Ultrasonically measured internal stresses can be reaffirmed by the computed values.

Authors are invited to publish their original research contributions, review articles, short communications, Ph.D. thesis one-page summary on topics related to ultrasonics including instrumentation, ultrasonic standards, propagation measurements, non-destructive evaluation & testing, transducers, underwater-acoustics, high power ultrasonics, etc.

— S. K. Jain
Chief Editor

J. Pure Appl. Ultrason. 42 (2020) pp. 59-65

Synthesis and spectroscopic characterization of Boehmite nanoparticles and its thermodynamic study

N.R. Pawar[1], Mrunal Pawar[2], R.D. Chavhan[3] and O.P. Chimankar[3]

[1]Department of Physics, Arts, Commerce and Science College, Maregaon-445 303, India
[2]St.Vincent Pallotti College of Engineering and Technology, Nagpur-441 108, India
[3]Department of Physics, RTM Nagpur University, Nagpur-440 033, India
*E-mail: pawarsir1@gmail.com

Boehmite nanofluids were synthesized by two step method. In this method Boehmite nano-powder was initially prepared and the powder was dispersed in methanol base fluid by magnetic stirrer method. The prepared nanopowder was characterized by X- ray diffraction (XRD), FTIR and Scanning electron microscopy (SEM). Average particle size has been estimated by using Debye-Scherrer formula. It was found to be about 50 nm. Nanofluids of Boehmite in methanol base fluid were prepared for various molar concentrations and their acoustical studies were made such that different types of interactions could be assessed. Thermo-acoustical parameters of this nanofluids system were computed from ultrasonic velocities, densities and viscosities at temperatures 293K, 298K, 303K, 308K and 313K at fixed frequency 5 MHz over the entire range of concentrations. The obtained results of present investigation have been discussed in the light of interactions between the Boehmite nanoparticles and the molecules of methanol based fluids.

Keywords: Boehmite nanoparticles; Sol-gel technique; Fourier transform infrared spectroscopy; Scanning electron microscopy, Zeta potential.

Introduction

Surface activity is a key aspect of nanomaterials. At the nanoscale dimensions, the material properties changes significantly differing completely from their bulk counterparts. Agglomeration and aggregation blocks surface area from contact with other matter. Only well dispersed or single dispersed particles allow the full beneficial potential of the matter[1-7]. As a result good dispersing reduces the quantity of nanomaterials needed to achieve the same effects. The quantization effect arises in nanometer because the overall dimensions of objects are comparable to the characteristics wave-length of fundamental excitations in materials[8].

The Nanofluids exhibits much greater properties as compared to base fluid. Boehmite nanoparticles have seen a flurry of research in recent years as nanotech researchers, engineers, and manufacturers discover its myriad applications across various fields of interest[9].

As with many nanoparticles, it must be handled with care to avoid issues of toxicity. Boehmite Nanoparticles exhibits high stability, high purity, good wear resistance and a small thermal expansion co-efficient. These traits make it ideal for applications across a wide range of domains, with more being uncovered by the research of academics and engineers.

$Al(NO_3)_3\ 9H_2O$ is the source of aluminum. 6.49 g of NaOH dissolved in 50 ml of distilled water and 20 g of $Al(NO_3)_3\ 9H_2O$ dissolved in 30 ml distilled water were used for preparation of boehmite nanofluids.

Nanoparticles are mixed with base fluid; some of the particles are remain suspended in the fluid. These suspended particles in the base fluid are considerably changes the transfer charac

The thermo-physical Properties of nanofluids depends upon the various factors like preparation methods, working temperature, particle size and shape, and volume fraction. Generallyxchanger, in grinding, machining and in boiler flue gas temperature reduction. They exhibit

enhanced thermal conductivity and the convective heat transfer coefficient compared to the base fluid[12-14]. Nanofluids also have special acoustical properties and in ultrasonic fields display additional shear-wave reconversion of an incident compressional wave; the effect becomes more pronounced as concentration increases[15-16].

Boehmite nanoparticles have seen a flurry of research in recent years as nanotech researchers, engineers and manufacturers discover its myriad applications across various fields of interest. As with many nanoparticles, it must be handled with care to avoid issues of toxicity. A common ingredient in non-nanoscale forms as an abrasive agent, nanopowder formulations of boehmite offer unique opportunities. As with many nanoparticles, boehmite has seen a surge of interest in its potential as a catalyst some research has found it to work as a highly efficient

It maintains exceptional strength even at high temperatures, making it a valuable subject in research of refractory materials. Some researchers suggest a role of boehmite nanoparticles in vaccines, though its unique properties have provoked interest and raised questions of its potential in a variety of nonmedical applications.

Experimental Details

Sol-gel processing

The various techniques such as physical, chemical, biological and hybrid techniques are available to synthesized nanomaterials in the form of colloids, clusters, powders, tubes, rods, wires, thin film *etc*. The techniques to be used upon the material of interest, type of nanomaterials, their size, quantity and morphology. Boehmite nanoparticles have been synthesized by sol-gel method[17]. In sol gel processing chemical solution converted into an integrated network called gel during this process metal alkoxides and metal chlorides are typically undergoing hydrolysis and poly condensation reactions. After a drying process, the liquid phase is removed from the gel. Mechanical properties of the synthesized sample may be increased by thermal treatment *i.e.* calcination.

Synthesis of Boehmite nanoparticles

Boehmite nanoparticles were synthesized by dissolving 6.49g of NaOH in 50 ml of distilled water. In the second step 20 g of $Al(NO_3)_3$ $9H_2O$ was prepared in 30 ml distilled water. $Al(NO_3)_3$ $9H_2O$ is the source of aluminum. Now Sodium hydroxide solution is added to aluminium solution at the rate 2.94 ml/min with vigorous stirring for 17 min[18]. Obtained milky mixture was subjected with ultrasonic bath for 3h at room temperature. Mixture filtered and washed with distilled water. The precipitate was kept in 220 degree temp for 10 h. The sample so obtained isoehmite nanoparticle. Finally it was grinded to get it in powdered form.

Characterization

X-Ray Diffraction (XRD) was obtained with a diffractometer 'PAN analytical,' Model: Xpert PRO, equipped with Cu $K\alpha_1$ radiation. Scanning Electron Microscopy (SEM) was made using a field emission JSM-7401F Scanning Electron Microscope. Infrared spectrum of absorption or emission of nanoparticles was obtained by Fourier Transform Infrared (FTIR) spectrophotometer Nicolet. Zeta potential of Boehmite nanofluids was measured by means Zeta Potential Analyzer. Thermal conductivity was measured by Thermal conductivity meter model DTC-300. Thermodynamic analysis of Boehmite nanofluids were studied by using pulser receiver.

Synthesis of Boehmite nanofluids

Two step methods is the most widely used method for preparing nanofluids. Nanoparticles, nanofibers, nanotubes or other nanomaterials used in this method are first produced as dry powders by chemical or physical methods. Then the nanosize powder will be dispersed into a fluid in the second processing step with the help of intensive magnetic force agitation, ultrasonic agitation, high shear mixing, homogenizing and ball milling and surfactants were used to enhance the stability of nanoparticles in nanofluids.

Nanofluids of Boehmite nanoparticles are produced in methanol base fluid by two step method using a magnetic stirrer for 30 min. Then the mixture is subjected to microwave heating till the reaction completes and the colour of the mixture may be changes. The obtained product is the Boehmite nanofluid[19].

Results and Discussion

X-Ray Diffraction (XRD)

Many techniques are used to identify the various

properties of nanomaterials. Some of the most important techniques are: XRD is a non-destructive versatile technique used to analyze the structure of crystalline materials and to identify the crystalline phases present in a material. It provides detail information about the chemical composition and crystallographic structure of natural and manufactured materials. In a crystalline solid, the constituent particles are arranged in regular periodic manner. An interaction of a particular crystalline solid with X-ray helps in investigation of its actual structure. Crystal is found to act as diffraction grating for X-ray and this indicates that the constituent particles in the crystal are arranged in planes at close distance in repeating patterns. The 2θ value corresponding to peak in the X-ray diffraction is an important tool to understand the properties of characterizes materials. In nano-materials number of atoms is very small. Nanoparticles cannot be considered as an infinite arrangement of atoms. In case of amorphous nanoparticles broad diffraction peaks are expected to occur similar to amorphous bulk solid materials. However, in case of nanoparticles atoms do not have ordered lattices, some changes in diffraction are to be expected as compared to single crystal. Nanoparticles do not have grain boundaries. It has been found that diffraction peaks in nanocrystalline particles are broadened compared to a single or polycrystalline solid of same materials. From XRD pattern, Debye Scherrer gives an equation to determine nanoparticles size as,

$$D = \frac{0.9\lambda}{\beta \cos\theta} \quad (1)$$

In above equation β is the broadening caused by nanoparticles size, θ is the Bragg's angle and λ is the wavelength of X-ray beam.

Figure 1 shows the XRD pattern of Boehmite nanoparticles reporting some Al and OH phases centred at 2θ = 15°, 28°, 40°, 50°, 65° and 72°. The XRD measurement carried out by using "PAN analytical" X-ray diffractometer keeping the parameter constant at start position [°2θ]: 10.0154 End Position [°2θ]: 89.9834, Step Size [°2θ]: 0.0170, Scan Step Time [s]: 5.7150, Scan Type: Continuous, Measurement Temperature [°C]: 25.00 Anode Material: Cu, K-Alpha1 [Å]: 1.54060. It is seen that the materials is well crystalline in nature and well agreed with standard JCPDS file number 021-1307. The estimate size of Boehmite nanoparticles using Debye Scherrer formula is found about 50 nm.

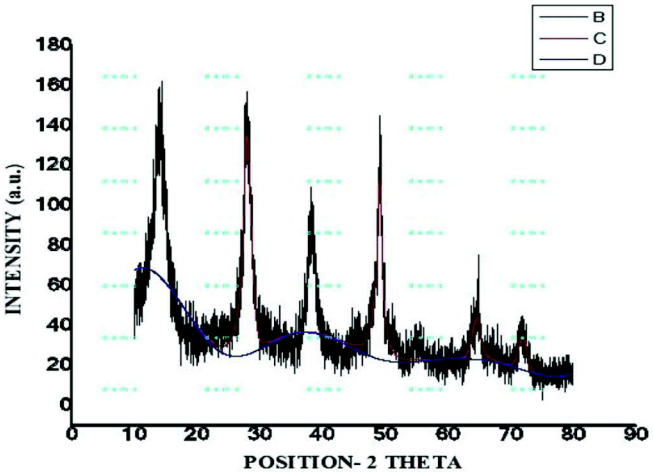

Fig. 1. X- ray diffraction pattern of Boehmite nanoparticles

Fourier Transform Infrared Spectroscopy (FTIR)

FTIR analysis indicated the vibrations of metal oxygen (M-O) groups. FTIR spectroscopy shows the degradation phases and absorption in different regions which indicates structural relationship between them. From figure 2, it is seen that the inorganic groups is gradually decomposed at 735.47 cm^{-1}, 1076.43 cm^{-1}, 3095.40 cm^{-1} 3311.81 cm^{-1}. Also the O-H absorption peak observed at 1402.45 cm^{-1}, 1648.95 cm^{-1}, 2893.02 cm^{-1} and a very weak band at about 3742.25 cm^{-1} is attributed due to the symmetrical stretching vibrations of the N-O group, which might have come from the nitrate of the starting material. The spectrum shows a peak at 735.47 cm^{-1}, which is due to the Al-O vibrations in the spinel block alumina structure.

Scanning Electron Microscopy (SEM)

SEM study is carried out to observe the overall surface morphology and crystallite sizes of the prepared nanomaterials. This material has been synthesis by sol-

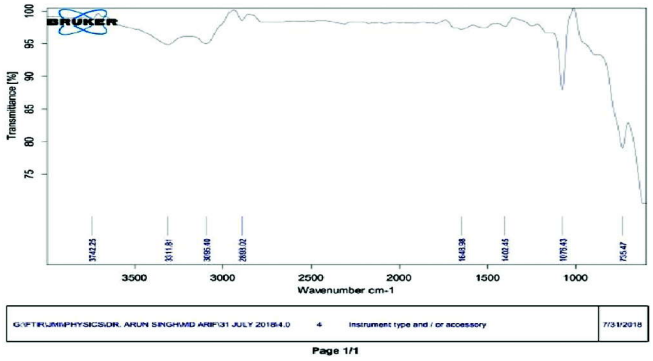

Fig. 2. FTIR spectra of Boehmite nanoparticles

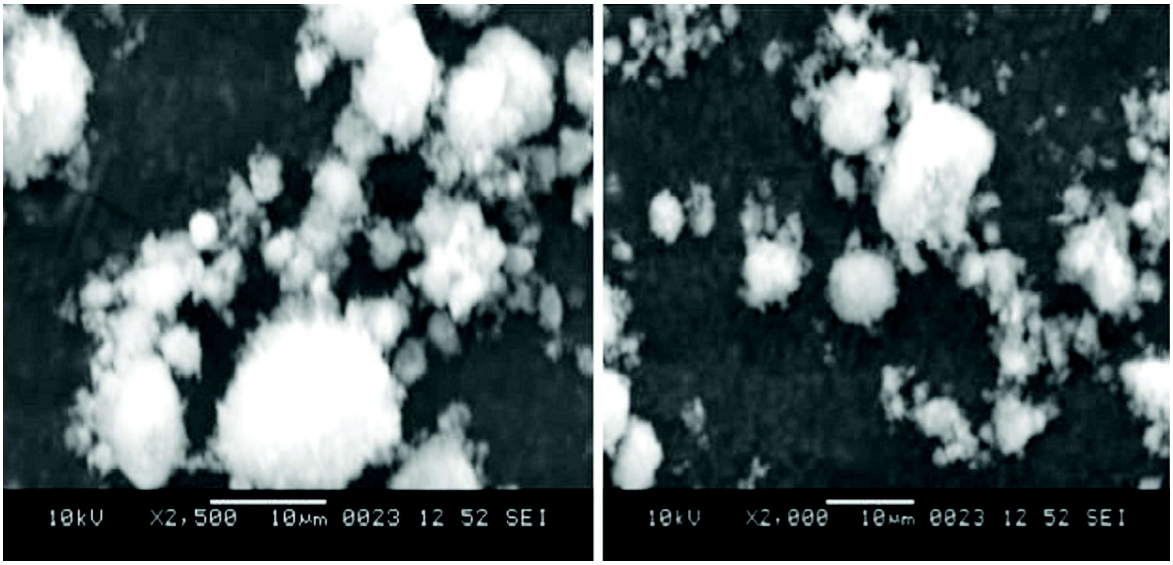

Fig. 3. SEM images of Boehmite Nanoparticles

gel method. From the SEM images are observed under 10 micrometer resolutions which show the foam like surface morphology as shown in Fig. 3. In the depicted images of Boehmite (AlOOH) nano-materials, it can be clearly seen that the micrograph crystallite sizes may vary from a 10 μm to few microns range if we magnifies further. The crystallites looks like having a sharp surface edge as well as crystalline grains and the particles foamlike morphology can be formed from highly agglomerated crystallites. Also it is confirmed that the crystallite sizes are nearly equal for all sample.

Zeta potential

Zeta potential of Boehmite nanofluids was measured by using Zeta potential analyser. It is the potential difference across phase boundaries between solids and liquids. It measure the electrical charge of nanoparticles that are suspended in liquid. It also measured the stability of the dispersion formed due to the reaction. It may be used to estimate the surface charge in the dispersion medium. It is the potential difference between the dispersion medium and dispersed particle. Zeta potential measurements is an important characterization method forsurface stability of nanofluids. The positive or negative values of zeta potential are necessary to ensure the stability of nanofluids. It is used to avoid the aggregation of nanoparticles in nanofluids by varying the stabilizar concentration or by surface modification. It is a measure of magnitude of charges on nanoparticles. Normally the higher values either positive or negative more than 30 indicates good stability. Zeta potentioal of

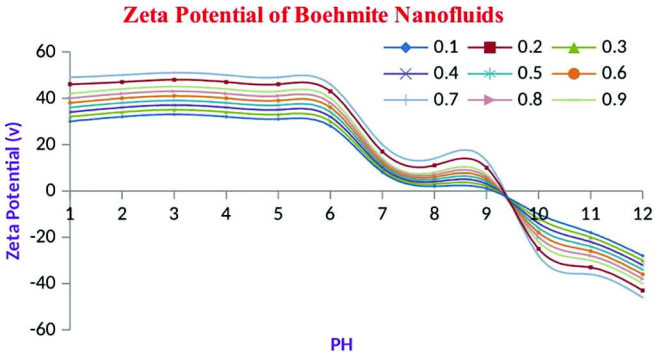

Fig. 4. Zeta potential of Boehmite nanofluids in methanol

Boehmite nanofluids in methanol with molar concentration are shown in Fig. 4. It is observed that zeta potential for molar concentration 0.2 and 0.7 have higher values indicating more stability of SiC nanofluids at these concentrations. Moreever it has less values for other molar concentration indicating less stability. From the graph the values of the zeta potential has values more than 30 either positive or negative for number of concentration showing more stability of synthesized nanofluids.

Thermo physical properties of nanofluids

Nanoparticles have great potential to improve the thermal transport properties compared to conventional particles fluids suspension. Thermo physical properties of the nanofluids are extremely important in the control for the industrial and energy saving perspectives because of their heat transfer behaviour. Now a days nanofluids

have gained significant attention due to its enhanced thermal properties. Presently researchers have great industrial interest in nanofluids.

Thermal Conductivity : Experimental studies show that thermal conductivity of nanofluids highly dependent on many factors such as particle volume fraction, base fluid material, particle shape and size, mixture combinations and slip mechanisms, surfactant, temperature and acidity of the nanofluid are effective in the thermal conductivity enhancement. Review of studies showed that the thermal conductivity increases by use of nanofluid compared to base fluid.

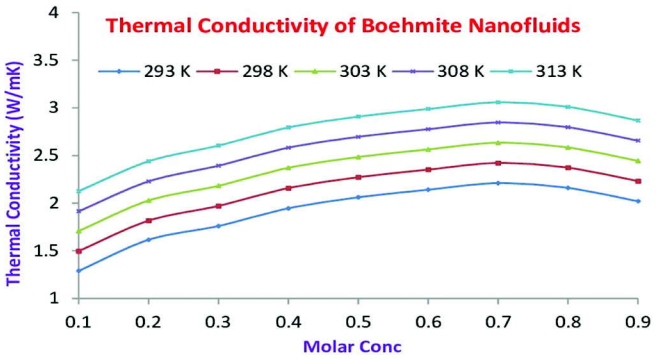

Fig. 5. Thermal conductivity of Boehmite nanofluids in methanol

Figure 5 shows the variation of thermal conductivity with molar concentration of Boehmite nanofluids in methanol. The results clearly show that the effective thermal conductivity of nanofluid increases with temperature. It has substantially higher value at molar concentration 0.2 and 0.7 indicating more stability of nanofluids because of high specific surface area and therefore more heat transfer surface between nanoparticles and fluids. The thermal conductivity enhancements are highly dependent on specific surface area of nanoparticle, with an optimal surface area for the highest thermal conductivity[20].

Sound velocity: Sound velocity gets increases with increasing the molar concentration of the Boehmite nanoparticles in methanol this shows that the physical parameters of the sample changes by increasing the molar concentration. Nanoparticles are disbursed in fluid medium which imparts sound velocity to the nanofluids. For Boehmite nanoparticle the velocity of the nanofluid is higher than methanol and also by increasing the molar concentration of the Boehmite nanoparticle the velocity gets maximum at 0.7 and then decreases, it is represented

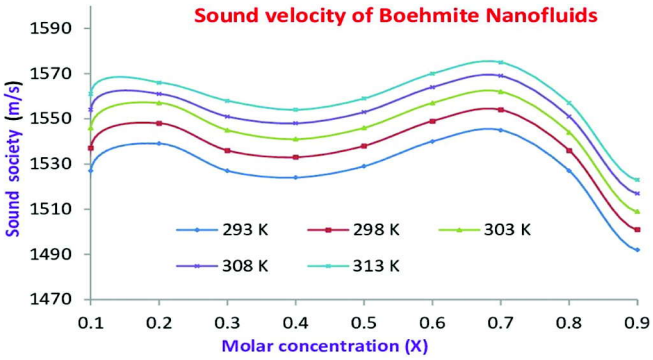

Fig. 6. Sound velocity of Boehmite nanofluids in methanol

in Fig. 6. The cause behind this increase of sound velocity with increase in molar concentration (x) may due to strong interaction between nanosize particle and micro sized fluid molecule.Sound velocity can be interpreted as the nanosize Boehmite particles have more surfaces to volume ratio and which can absorb more methanol molecules on its surface, which enhances the sound velocity. Brownian motion is the erratic and constant motion of suspended nanoparticles in fluid. Motion of the particle becomes more rapid with increase in temperature of the medium which enhances sound velocity of the nanofluid[21].

Isothermal Bulk Modulus: Isothermal bulk modulus is a thermodynamic quantity, it is necessary to specify how the temperature varies during compression. It is a measure of increase in pressure to the resulting decrease of the volume. For a nanofluid only the bulk modulus is meaningful. The variation of isothermal Bulk modulus with molar concentration of Boehmite nanoparticles in methanol based nanofluids is given in Fig. 7.

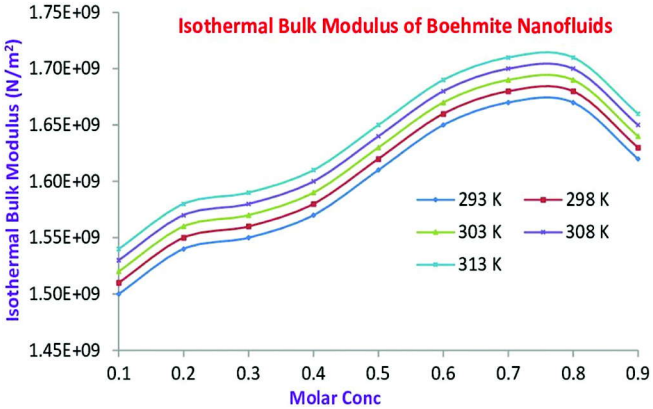

Fig. 7. Isothermal bulk modulus of Boehmite nanofluids in methanol

The variation clearly shows that isothermal bulk modulus (Bi) increases with increase in molar concentration with a remarkable peak at 0.7. It exhibits similar trends as that of sound velocity. Its non linear variation indicates strong interactions between Boehmite nanoparticles and molecules of methanol showing more disbursing tendency of the Boehmite nanoparticles in nanofluids in order to obtained stability[22].

Volume expansivity: Volume expansivity is the fractional increase in volume of a nanofluid per unit rise in temperature. It is observed that volume expansivity decreases with increase in molar concentration of Boehmite nanoparticles nanofluids due to stability and Brownion motion of nanoparticles in nanofluids[23]. As it is depends on internal pressure and isothermal compressibility it shows their resultant effects. Its variation with molar concentration is given in Fig. 8.

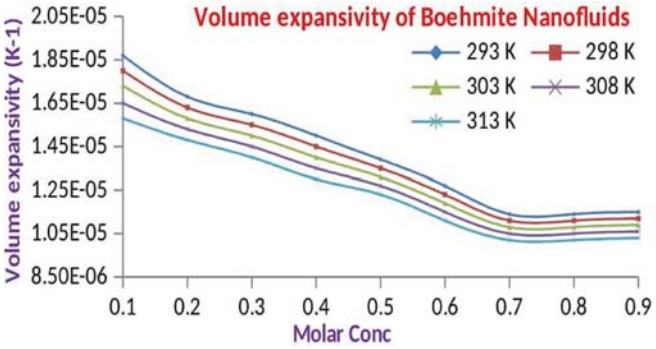

Fig. 8. Volume expansivity of Boehmite nanofluids in methanol

Conclusion

1. Besides thermal conductivity effect, future research should consider other properties, especially viscosity and wettability, and examine systematically their influence on flow and heat transfer. An in depth understanding of the interactions between particles, stabilizers, the suspending liquid and the heating surface will be important for applications.
2. Pioneering nanofluids research has inspired physicists, chemists and engineers around the world.
3. Characterization of Boehmite nanoparticles via XRD and SEM showed that nanocrystalline Boehmite are formed.
4. FTIR spectra of the Boehmite nanoparticles have revealed strong absorption bands with a very small variation.
5. Enhancement in thermal conductivity, sound velocity isothermal bulk modulus and decrement in volume expansivity of Boehmite nanofluids is due to the stability of Boehmite nanoparticles in dispersion medium and Brownian motion of the nanoparticles in the nanofluids

References

1 **Kumar D.H., Patel H.E., Kumar V.R.R., Sundararajan T., Pradeep T.** and **Das S.K.,** Model for heat conduction of nanofluids, *Phys. Rev. Lett.,* **94**(14) (2004) 1-3.

2 **Rajagopalan S., Sharma S.J.** and **Nanotkar V.Y.,** Ultrasonic characterization of silver nanoparticles, *J,. Metast. Nanocryst. Mat.,* **23** (2005) 271-274.

3 **Peng C., Zhang J., Xiong Z., Zhao B.** and **Liu P.,** "Fabrication of porous hollow γ-Al_2O_3 nanofibers by facile electro spinning and its application for water remediation", *Microp. Mesop. Mat.,* **215** (2015) 133-142, (2002) 1896-1899. doi:10.1557/JMR.2002.0281.

4 **Zhan X., Honkanen M.** and **Leva E.,** Transition alumina nanoparticles and nanorods from boehmite nanoflakes. *J Crystal Growth.* **310**(30) (2008) 3674-3679.

5 **Guo W., Xiao H., Xie W., Hu J., Li Q.** and **Gao P.,** A new design for preparation of high performance recrystallized silicon carbide. *Ceramics Int.* **38** (2012) 2475-2481.

6 **Chavhan R.D., Abhranil Banerjee, Mrunal Pawar, Chimankarand O.P.** and **Pawar N.R.,** Synthesis and ultrasonic characterization of boron nitride nano suspension inorganic base fluids, *J. Pure Appl. Ultrason.* **41** (2019) 80-83.

7 **Chavhan R.D., Abhranil Banerjee, MrunalPawar, Chimankar O.P., Dhobleand S.J.** and **Pawar N.R.,** Synthesis and ultrasonic characterization of silicon carbide nano suspension inorganic base fluids, *JETIR,* **6**(4) (2019) 309-318.

8 **Thirumaran S.** and **George D.,** *Arpan J Eng. Appl. Sci,* **4**(4) (2009).

9 **Wang B.X., Zhou L.P.** and **Peng X.F.,** A fractal model for predicting the effective thermal conductivity of liquid with suspension of nanoparticles, *Int. J. Heat Mass Transfer,* **46**(14) (2003) 2665-2672.

10 **Chooi S.U.S.** and **Eastman, J.A.,** Enhancing thermal conductivity of fluids with nanoparticles, *International mechanical engineering congress and exhibition,* San Francisco, CA, (1995).

11 **Das S.K., Chooi S.U.S.,Yu W.** and **Pradeep T.,** Naofluids: Science and Technology, *John Wiley and Sons, Inc,* (2008).

12 **Mishra G., Verma S.K., Singh D., Yadawa P.K.** and **Yadav R.R.,** Synthesis and ultrasonic characterization of Cu/PVP nanoparticles-polymer suspensions, *Open Journal of Acoustics,* **1**(1) (2011) 9-14.

13 **Puiso J., Jakevicius L., Macioniene I., Salmskiene J.** and **Jonkuviene D.**, Nanobiotechnology of silver nanoparticles, *KAUNO Technologijos universities* (1922).

14 **Singh A.K.,** Thermal conductivity of nanofluids, *Def. Sci. J.,* **58**(5) (2008).

15 **Wang B.X., Zhou L.P.** and **Peng X.F.,** A fractal model for predicting the effective thermal conductivity of liquid with suspension of nanoparticles, *Int. J. Heat Mass Transfer,* **46**(14) (2003) 2665-2672.

16 **Hyun-Lee L., Jong-Kyu K., Sang-Nam L.** and **Yong-Heack K.,** Consisten heat transfer analysis for performance evaluation of multichannel solar absorbers. *Solar Energy.* (2012) 1576-1585.

17 **Zhan X., Honkanen M.** and **Leva E.,** Transition alumina nanoparticles and nanorods from boehmite nanoflakes. *J. Crystal Growth*, **310**(30) (2008) 3674-3679.

18 **Yu W.** and **Xie H.,** A review of nanofluids: preparation, stability mechanisms and applications, *J. Nanomaterials,* **2012** (2011) 1-17.

19 **Lee S., Choi S.U.S., Li S.** and **Eastman J.A.,** Measuring thermal conductivity of fluids containing oxide nanoparticles, *J. Heat Transfer,* **121** (1999) 280-289.

20 **Pandey V., Mishra G., Verma S.K., Wan M.** and **Yadav R.R.,** Synthesis and ultrasonic investigations of CuO-PVA nanofluid, *J. Mater Sci. Appl.,* **3** (2012) 664-668.

21 **Singh M.,** Behaviour of isothermal bulk modulus of nanomaterials under the effect of temperature, *Mat. Sci.,* (2016) Corpus ID: 137785098.

22 **Pawar N.R., Chimankar O.P., Dhoble S.J.** and **Chavhan R.D.,** Synthesis, Thermal conductivity and characterization of alpha-Alumina (α-Al_2O_3) nano particles by Non-destructive ultrasonic technique, *J. Acoust. Soc. India,* **43**(3) (2016) 16.

J. Pure Appl. Ultrason. 42 (2020) pp. 66-71

Temperature and frequency dependence of acoustic attenuation in pure semiconductors

Sanjay H. Bagade

Department of Physics, Bajaj College of Science, Wardha-442 001, India
*E-mail: sanjaybagade8@gmail.com

Real solids show a deviation from perfectly elastic behavior and exhibit anharmonicity due to existence of zero-point energy, owing to which, a stress wave in the form of high frequency acoustic wave, travelling through it, gets attenuated. In the present work, some acoustic properties of pure semiconductors germanium and silicon, are investigated within temperature range 73-293 K, by making use of second and third order elastic constants. Assuming a temperature dependent non-linearity parameter D_L, D_S, the acoustic wave attenuation 'A' is calculated for longitudinal waves of frequency 286 MHz and 495 MHz and for shear waves of 495 MHz, propagating in pure germanium and silicon. The Akhieser losses leading to attenuation are attributed mainly to phonon-phonon interactions within the solid. Attenuation of high frequency waves is found to be strongly temperature and frequency dependent. Theoretically calculated values of attenuation 'A' show good agreement with experimental values obtained earlier.

Keywords: Acoustic wave attenuation, longitudinal waves, shear waves, elastic constants.

Introduction

The investigations related to progress of mechanical waves through solids are useful technique to study various properties of the solid materials[1]. Longitudinal and shear waves progress with undiminished amplitude as well as intensity if the solid is perfectly elastic, where the Hooke's law is obeyed to perfection. Since harmonic approximations are not valid for real solids, stress waves are attenuated even in absence of any dissipating mechanisms. Attenuation is thus a direct consequence of anharmonicity in solids[2-4].Using the "picosecond ultrasonic technique" attenuation of the acoustic waves was studied and the phenomenon of attenuation was found to be strongly influenced by the anharmonicity in the semiconductor crystal GaAs[5]. Phonon-electron interactions as a possible cause of acoustic wave attenuation in piezoelectric semiconductors have been investigated besides the losses due to anharmonicity[6].

Due to an harmonic nature of the inter atomic forces in real solids, the acoustic waves travelling through it interacts with thermal lattice waves and gets attenuated[7]. If $\Omega\tau >> 1$, where Ω is angular frequency of acoustic waves and τ the relaxation time of thermal phonons, the acoustic waves interact directly with individual lattice phonons. This corresponds to a case where wavelength of the wave is much less than mean free path of the thermal phonons. This condition is satisfied for very high frequency acoustic waves travelling through solids at low temperatures[8].

Studies related to attenuation of high frequency acoustic waves in semiconductors has always been a matter of interest for researchers due to its vast applications and major initial contributions in this field had come from experimental works done by Mason and Bateman[9-18]. The failure of harmonic oscillator theory to explain the experimental results about attenuation of waves, led various workers to modify it. Gruneisen and Mason were perhaps the first to make allowance for 'anharmonicity' by assuming a temperature dependent non-linearity parameter D, in calculation of acoustic wave attenuation[12,16-18]. D is a function of second and third order elastic constant of solid under consideration and is also temperature dependent. Inclusion of temperature dependency of non-linearity parameter D

in calculation of the acoustic wave attenuation, led to fairly good agreement between the experimental work and theoretical calculations[15-18]. Attenuation of high frequency ultrasonic waves in semiconductor silicon had been investigated before[17]. Ultrasonic attenuation is found to be influenced by the thermal conductivity of solids and the responsible cause of attenuation is phonon-phonon interaction[25]. In the present work the attenuation of longitudinal waves of frequency 286 MHz and 495 MHz and shear waves of frequency 495 MHz progressing through pure silicon and germanium are calculated. The theoretically calculated values of attenuation A are compared and found to be in good agreement with the experimental values obtained by various researchers including W.P. Mason[13-18].

Theory

When longitudinal or shear waves propagate through solids, the attenuation of the waves is caused due to thermo elastic effect. In this case alternate regions of compression and rarefaction are set up within the solid, which differ in temperature. The temperature gradient thus created, give rise to the heat energy flow, resulting in energy dissipation in solids, and hence leads to attenuation of the longitudinal waves as well as shear waves. The attenuation for longitudinal waves in this case is given as in[2-4, 7],

$$\alpha = \frac{1}{2V_L}\frac{\Delta m}{m_0}\left[\frac{\omega^2\tau}{1+\omega^2\tau^2}\right] Np \text{ cm}^{-1} \quad (1)$$

where m_0 is the un-relaxed modulus of elasticity of the solid, Δm is the increment in modulus of elasticity, ω is the angular frequency, τ is the relaxation time given by $\tau = \psi / \rho C_v V_L^2$, Ψ, ρ and C_v are the thermal conductivity, density and specific heat capacity of solid. V_L is the velocity of propagation of the longitudinal wave through the solid, which is given as in[20-21].

$$V_L = \left[\frac{m_0}{\rho}\right]^{\frac{1}{2}} \quad (2)$$

Therefore, attenuation α becomes

$$\alpha = \frac{1}{2\rho V_L^3}\Delta m\left[\frac{\omega^2\tau}{1+\omega^2\tau^2}\right] Np \text{ cm}^{-1} \quad (3)$$

The increment in modulus of elasticity is given as

$$\Delta m = 3\sum_i E_0(\gamma_i^1)^2 - \gamma_{av}^2 C_v T \quad (4)$$

where E_0 is the average thermal energy, γ_i^1 and γ_{av} are the values of the Gruneisen constant, and the average value of Gruneisen constant for longitudinal waves along the [100] axis.

Using Eqs. (4) and (3), the attenuation of longitudinal waves in solid becomes

$$\alpha = \frac{1}{2\rho V_L^3}\times\left[3\sum_i E_0(\gamma_i^1)^2 - \gamma_{av}^2 C_v T\right]\times\left[\frac{\omega^2\tau}{1+\omega^2\tau^2}\right] Np \text{ cm}^{-1} \quad (5)$$

$$\alpha = \frac{E_0\left(\frac{D}{3}\right)}{2\rho V_L^3}\left[\frac{\omega^2\tau}{1+\omega^2\tau^2}\right] Np \text{ cm}^{-1} \quad (6)$$

where $D = \frac{3}{E_0}\left[3\sum_i E_0(\gamma_i^1)^2 - \gamma_{av}^2 C_v T\right]$ is the non-linearity parameter for the propagating longitudinal waves. If n is the statistical frequency of the Gruneisen constant of longitudinal waves along [100] axis, the non-linearity parameter D is expressed as

$$D_L = 3\left[\frac{3\sum_i (\gamma_i^1)^2 n_i}{\sum_i n_i} - \frac{\gamma_{av}{}^2 C_v T}{E_0}\right] \quad (7)$$

Finally, the attenuation of the longitudinal waves in terms of dB cm^{-1} is obtained[12-15, 17].

$$\text{Attenuation} = A = 8.686 \times \alpha \text{ (dB cm}^{-1}\text{)} \quad (8)$$

For pure shear wave propagation through solids, the average value of Gruneisen constant γ_{av} along the [100] axis is zero. Hence the non-linearity parameter D for shear wave propagation can be obtained by replacing γ_i^1 by γ_i^5, Gruneisen constant for shear waves, γ_{av} by zero in Eq. (7). The non-linearity parameter D for shear wave is

$$D_S = 3\left[\frac{3\sum_i (\gamma_i^5)^2 n_i}{\sum_i n_i}\right] \quad (9)$$

Further replacing longitudinal velocity V_L by shear velocity V_S in Eq. (6), α can be found and hence using Eq. (8), attenuation $'A'$ for shear waves can be calculated.

Parameters used for calculations for germanium and silicon

Table 1 and Table 2 respectively give the various parameters used for calculation of attenuation in semiconductor material germanium and silicon. Parameters reported are density ρ, the average thermal energy E_0, specific heat capacity at constant volume C_v, the longitudinal wave velocity V_L, the shear wave velocity V_S, the average Gruneisen constant γ_{av}, $\sum_i (\gamma_i^5)^2 n_i$ for shear waves, $\sum_i (\gamma_i^1)^2 n_i$ for the longitudinal waves along [100] axis for various temperatures[10, 21-24].

Results and Discussion

The theoretically calculated values of non-linearity parameter D_L and the attenuation *A(T)* for longitudinal waves of frequency 286 MHz and 495 MHz, travelling along [100] axis in germanium and silicon, as well as, the experimentally obtained values of D_L and attenuation *A(E)* by W.P. Mason are reported in Table 3 and Table 4 respectively. Similarly D_S and attenuation A for shear waves of frequency 495 MHz along [100] axis in pure germanium and silicon are given in table 5. A good agreement is observed between the theoretically calculated values of D_L, D_S and A, using the temperature dependent second and third order elastic constants, with

Table 1 – For germanium

Temperature K	ρ gm cm^{-3}	$E_0 * 10^7$ erg	$C_v * 10^7$ erg gm^{-1} K^{-1}	$V_S * 10^5$ cm s^{-1}	$V_L * 10^5$ cm s^{-1}	γ_{av}	$\sum_i (\gamma_i^1)^2 n_i$	$\sum_i (\gamma_i^5)^2 n_i$
73	5.335	14.80	0.65	3.576	4.959	0.830	34.68	2.52
113	5.333	51.82	1.11	3.572	4.954	0.779	32.92	3.15
153	5.331	101.5	1.38	3.568	4.947	0.760	31.43	3.20
193	5.328	160.1	1.52	3.563	4.942	o.754	31.14	3.36
233	5.323	223.1	1.61	3.558	4.935	0.748	30.56	3.38
293	5.320	322.8	1.68	3.551	4.920	0.746	29.34	3.99

Table 2 – For silicon

Temperature K	ρ gm cm^{-3}	$E_0 * 10^7$ erg	$C_v * 10^7$ erg gm^{-1} K^{-1}	$V_S * 10^5$ cm s^{-1}	$V_L * 10^5$ cm s^{-1}	γ_{av}	$\sum_i (\gamma_i^1)^2 n_i$	$\sum_i (\gamma_i^5)^2 n_i$
73	2.325	4.106	0.217	5.868	8.4865	0.630	16.68	1.244
113	2.324	20.16	0.598	5.866	8.4836	0.579	16.92	1.580
153	2.324	51.78	0.967	5.864	8.4785	0.560	16.43	1.587
193	2.323	96.39	1.246	5.863	8.4723	o.554	16.14	1.638
233	2.322	150.5	1.443	5.860	8.4653	0.548	15.56	1.658
293	2.320	244.6	1.635	5.856	8.4524	0.503	14.34	1.845

Table 3 – For germanium

Temperature K	longitudinal waves: frequency 286MHz				longitudinal waves : frequency 495 MHz			
	D_L (T)	D_L (E)	A (T) dB cm^{-1}	A(E) dB cm^{-1}	D_L (T)	D_L (E)	A (T) dB cm^{-1}	A(E) dB cm^{-1}
73	2.325	4.106	0.217	5.868	8.4865	0.630	16.68	1.244
113	2.324	20.16	0.598	5.866	8.4836	0.579	16.92	1.580
153	2.324	51.78	0.967	5.864	8.4785	0.560	16.43	1.587
193	2.323	96.39	1.246	5.863	8.4723	o.554	16.14	1.638
233	2.322	150.5	1.443	5.860	8.4653	0.548	15.56	1.658
293	2.320	244.6	1.635	5.856	8.4524	0.503	14.34	1.845

Table 4 – For silicon

Temperature K	longitudinal waves: frequency 286MHz				longitudinal waves : frequency 495 MHz			
	D_S (T)	D_S (E)	A (T) dB cm^{-1}	A(E) dB cm^{-1}	D_S (T)	D_S (E)	A (T) dB cm^{-1}	A(E) dB cm^{-1}
73	3.211	3.416	0.170	0.243	3.260	3.536	0.290	0.547
113	4.224	4.562	0.282	0.458	4.343	4.648	0.850	1.024
153	4.449	4.896	0.433	0.585	4.669	4.986	1.199	1.342
193	5.018	5.066	0.544	0.624	5.124	5.314	1.345	1.565
233	5.302	5.625	0.629	0.698	5.435	5.768	1.624	1.844
293	5.345	5.676	0.720	0.755	5.658	5.887	1.964	2.225

Table 5 – Shear waves in Ge and Si

Temperature K	Shear wavesof 495 MHz in Si				Shear waves 495 MHzin Ge			
	D_S (T)*	D_S (E)*	A (T) dB cm^{-1}	A(E) dB cm^{-1}	D_S (T)	D_S (E)	A (T) dB cm^{-1}	A(E) dB cm^{-1}
73	1.086	1.244	0.360	0.400	1.986	2.244	0.651	0.746
113	1.194	1.581	0.518	0.524	2.194	2.881	0.863	0.954
153	1.401	1.587	0.588	0.703	2.401	3.587	1.122	1.328
193	1.413	1.683	0.617	0.800	2.413	3.683	1.257	1.508
233	1.718	1.689	0.635	0.822	2.982	3.932	1.346	1.684
293	1.978	2.007	0.656	0.834	3.1978	3.994	1.688	1.884

*(T) refers to the theoretically calculated values of non-linearity parameter D_L, D_S and attenuation A and

*(E) refers to the experimentally obtained values of D_L, D_S and attenuation A

those experimentally obtained[13-19]. The variation of attenuation A with temperature for longitudinal waves in germanium and silicon is shown in Fig. 1 and Fig. 2 respectively. Shear wave attenuation is shown in Fig. 3.

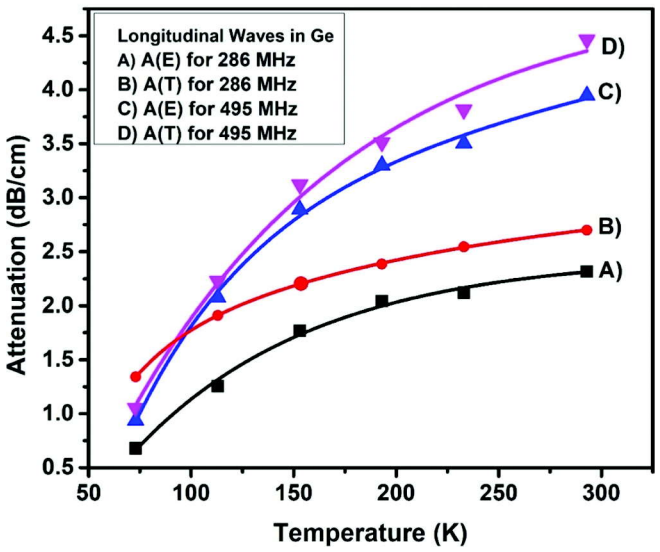

Fig. 1. Attenuation of longitudinal waves in germanium.

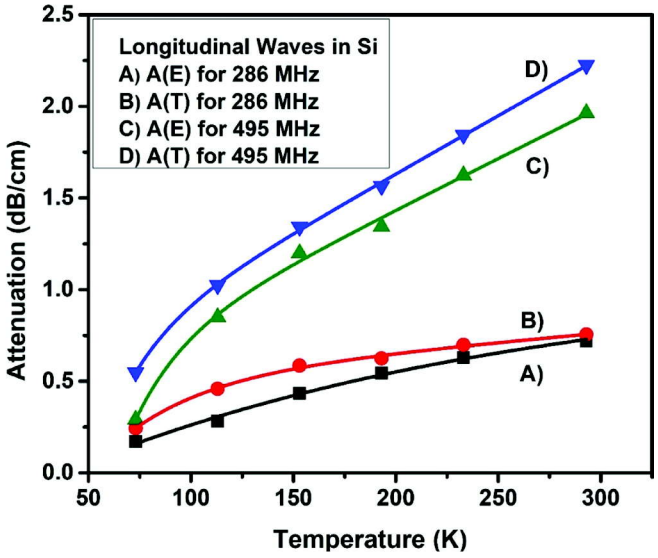

Fig. 2. Attenuation of longitudinal waves in silicon.

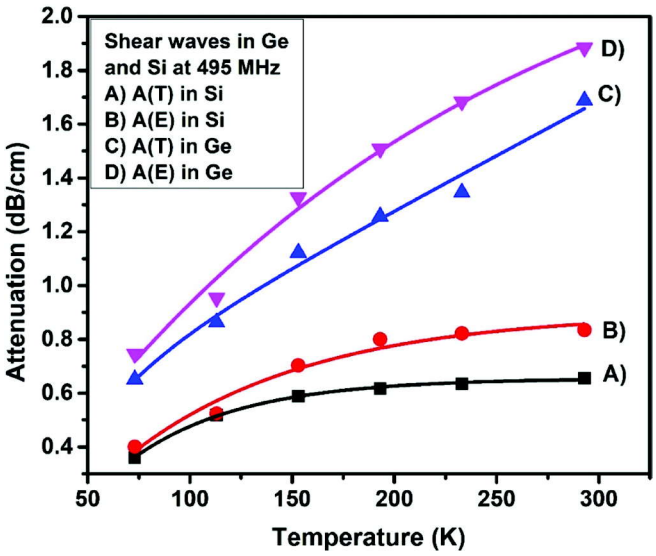

Fig. 3. Attenuation of shear waves in germanium and silicon.

The non-linearity parameter D_L shows an increase with the temperature, for the longitudinal waves in both germanium and silicon, which may be due to decrease in value of the average Gruneisen constant γ_{av}. The value of D_S for shear waves also shows an increase with the temperature. The Akhieser losses leading to attenuation in pure semiconductor are attributed mainly to phonon-phonon interactions and the thermo elastic losses due to thermal conduction between the compressed and expanded part of the solid medium, as the longitudinal and shear acoustic wave progress through it. The contribution of the latter part to wave attenuation is found to be negligible.

From the graph it is evident that the attenuation of acoustic waves in pure semiconductor is strongly temperature dependent and it goes on increasing with the temperature, both in case of longitudinal and shear waves. Also, for the longitudinal and shear waves, it is seen that the frequency of acoustic waves influences the attenuation of waves. The waves of larger frequency suffer large attenuation as compared to low frequency waves. From the calculations it is evident that the magnitude of attenuation A for longitudinal waves is greater than that for the shear waves. Hence for same frequency and temperature the longitudinal waves are more attenuated as compared to the shear waves. Calculations also show that the magnitude of attenuation for given temperature and given frequency of waves is greater in germanium as compared to attenuation in silicon.

Conclusion

Attenuation in pure semiconductor is both temperature and frequency dependent. Higher attenuation is observed for higher temperature and higher frequency of the waves. For same frequency and temperature, the longitudinal waves are more attenuated as compared to the shear waves. The semiconductor germanium material provides higher attenuation of the longitudinal as well as shear acoustic waves propagating through it, as compared to silicon. As a result, it can be more preferred as an attenuating medium in various industrial and technological applications

References

1 **Einspruch N.,** Ultrasonic effects in semiconductors, *Solid State Phys.,* **17** (1965) 217-268.

2 **Mason W.P.,** Ultrasonic attenuation due to lattice-electron interaction in normal conducting metals, *Phys. Rev.* **97** (1955) 557.

3 **Mason W.P.,** Piezoelectric Crystals and their Applications to Ultrasonics, *(Van Nostrand: New York)* (1950).

4 **Mason W.P.,** Physical Acoustics, edited by W.P. Mason and R.N. Thurston *(Academic Press: New York)* (1964).

5 **Maris H.J.,** Physical Acoustics, edited by W.P. Mason and R.N. Thurston *(Academic Press, New York)* (1971).

6 **Akhiezer A.J.,** On the absorption of sound in solids, *J. Phys. (Moscow)*. **1** (1939) 277-287.

7 **Morse R.W.,** Ultrasonic attenuation in metals by electron relaxation, *Phys. Rev.* **97** (1955) 1716.

8 **Kor S.K.** and **Singh R.K.,** Ultrasonic attenuation in normal valence semiconductors, *Acustica,* **80** (1994) 83-87.

9 **Barrett H.H.** and **Holland M.G.,** Critique of current theories of Akhieser damping in solids, *Phys. Rev. B,* **1** (1970) 2538-2544.

10 **Nava R., Vecchi M., Romero J.** and **Fernandez B.,** Akhiezer damping and the thermal conductivity of pure and impure dielectrics, *Phys. Rev. B,* **14** (1976) 800-807.

11 **Mason W.P.** and **Bateman T.B.,** Ultrasonic wave propagation in pure silicon and germanium, *J. Acoust. Soc. Am.,* **36** (1964) 645-655.

12 **Mason W.P.,** Effect of Impurities and phonon processes on the ultrasonic attenuation of germanium, crystal quartz and Silicon, *In:* W.P. Mason, Ed., Physical Acoustics, *(Academic Press, New York)* **III B** (1965) 235-285.

13 **Joharapurkar D.N., Rajagopalan S.** and **Basu B.K.,** Ultrasonic velocity, attenuation and nonlinearity constant in pure and Cd-Doped KCl, *Phys. Rev. B,* **37**(6) (1988) 3101-3104.

14 **Nandanpawar M.** and **Rajagopalan S.,** Ultrasonic attenuation in copper and the temperature dependence of the nonlinearity parameter, *Phys. Rev. B,* **18**(10) (1988) 5410-5412.

15 **Joharapurkar D.N., Gerlich D.** and **Breazeale M.,** Temperature dependence of elastic nonlinearities in single crystal gallium arsenide, *J. Appl. Phys.,* **72** (1990) 2202-2208.

16 **Mason W.P.** and **Bateman T.B.,** Relation between third-order elastic moduli and the thermal attenuation of ultrasonic waves in non-conducting and metallic crystals, *J. Acoust. Soc. Am.,* **40**(4) (1966) 852-862.

17 **Bagade S.H.** and **Ghodki V.M.,** Study of high frequency acoustic wave attenuation in semiconductor silicon at different temperatures, *J. Pure Appl. Ultrason.,* **35** (2013) 56-58.

18 **Achenbach J.D.,** Wave propagation in elastic solids, 1st edition, *North-Holland* (1984).

19 **Knopoff L.** and **Gordon J.F.,** Attenuation of small amplitude stress waves in solids, *Rev. Mod. Physics,* **30** (1958) 1178.

20 **Shackelford J.F.,** Introduction tomaterial science for engineers, 3rd ed. *(Macmillan)* (1992).

21 **Weast R.C.,** Hand book of chemistry and physics, *CRC Press (Princeton Uni.)* (1988).

22 **Hiki Y.J.,** Higher order elastic constants of solids, *Annu. Rev. Mater. Sci.,* **11** (1981) 51-73.

23 **Legrand R., Huynh A., Jusserand B., Perrin B.** and **Lemaître A.,** Direct measurement of coherent subterahertz acoustic phonons mean free path in GaAs, *Phys. Rev. B*. **93** (2016) 184304.

24 **Gokhale V.** and **Rais-Zadeh M.,** Phonon-electron interactions in piezoelectric semiconductor bulk acoustic wave resonators, *Sci. Rep*. **4** (2015) 5617.

25 **Tripathi S., Agarwal R.** and **Singh D.,** Size dependent ultrasonic and thermophysical properties of indium phosphide nanowires, *Z. Naturforsch*. **75** (2020) 373-380.

J. Pure Appl. Ultrason. 42 (2020) pp. 72-77

Acoustic and refractive behaviour of the binary mixture of 1-butyl-3 methylimidazolium tetrafluoroborate with 1-alkanol at 298.15 to 313.15K

Ankit Gupta[#], V. S. Gangwar, Ashish Kumar Singh, S. K. Singh and R.K. Shukla[*]

Department of Chemistry, V.S.S.D. College, Kanpur-208 002, India
*E-mail: rajeevshukla47@rediffmail.com

Densities, refractive indices and speeds of sound and their excess properties for 1-butyl-3-methylimidazolium tetrafluoroborate [Bmim][BF4] with 1-pentanol over the entire range of mole fraction are reported at temperatures ranging from 298.15 K to 313.15 K and atmospheric pressure. Isentropic and excess isentropic compressibility for ionic liquids with 1-alcohols were calculated from the experimental results. The excess values are fitted to the Redlich-Kister polynomial equation to estimate the binary coefficients and standard error between the experimental and calculated values. The measured speeds of sound were compared to the values obtained from Schaaffs' collision factor theory, Jacobson's intermolecular free length theory of solutions and Nomoto's relation. In addition, the experimentally obtained refractive indices were compared to the calculated values using Lorentz-Lorenz, Dale-Gladstone and Eykman mixing rules. The theoretical results obtained from these relations fairly agrees within the experimental precision. Further, the molecular interactions involved in IL binary mixture system were studied.

Keywords: Density, refractive index, speed of sound, ionic liquids, binary mixture.

Introduction

Ionic liquids (ILs) have recently emerged as environment friendly solvents for their use in the industrial manufacture of chemicals. In the past decade, ILs have been increasingly used for diverse applications such as organic synthesis, catalysis, electrochemical devices, and solvent extraction of a variety of compounds[1-4]. The interest in ILs was initiated because of their advantageous physico-chemical properties. ILs are composed of cations and anions having a low melting point. The physico-chemical properties of the ILs can be tuned by changing the cation or the anion. Thus, novel solvents can be formed and can be used for a specific application which cannot be done with the use of conventional organic solvents. The information regarding the thermo-physical properties of pure ILs as well as their mixtures with other compounds is essential for the design and development of equipment for commercial applications. [Bmim][BF4] is most efficient in the removal of di-benzothiophene (DBT) containing liquid fuels[5]. Pentanol is used as co-solvent in the petroleum industry to increase the selectivity and solvent power for extracting aromatic hydrocarbons.

Similar study has been carried out by us[6-8] and many other workers for non ionic liquids, particularly hydro carbons, cyclic compound, to validate these theoretical models and also the solvent - solvent interactions present in liquid mixture.

The present work is aimed at studying the molecular interactions in the binary mixture of the IL 1-butyl-3-methylimidazolium tetrafluoroborate [Bmim][BF4] with 1-alconol. Isentropic and excess isentropic compressibility's for ionic liquids with 1-alconols were calculated from the experimental results. Excess and deviation properties were further correlated using the Redlich-Kister polynomial eqation[9]. The measured speeds of sound were compared to the values obtained from Schaaffs' collision factor theory(CFT)[10], Jacobson's intermolecular free length theory(FLT)[11-12] of solutions and Nomoto's relation (NR)[13]. In addition, the experimentally obtained refractive indices were compared to the calculated values using Lorentz-Lorenz[14], Dale-Gladstone[15] and Eykman mixing rules[16]. Experimental

values and excess thermodynamic properties of IL systems allow researchers to draw information on the structure and interactions of liquid mixtures. The corresponding excess molar volume and excess isentropic compressibility and coefficients of thermal expansion were calculated. Furthermore, the Redlich and Kister (R-K) polynomial was used to obtain the coefficients and to estimate the standard deviations for the calculated excess and deviation properties. Moreover, the effect of the alkyl chain in ILs, chain length of 1-alkanol and the temperature on the excess and deviation properties are investigated.

Experimental

Materials : [Bmim][BF4] (mass fraction, 0.99) is procured from Merck, Germany, and is used without further purification. 1-Pentanol (mass fraction 0.97) is procured from Sigma-Aldrich, USA, and is purified by the fractional distillation method under reduced pressure. The water content is checked by conductometric titration with platinum electrode. The purity of the chemicals was ascertained by comparing the experimental values of density, refractive index and speed of sound, at temperatures T = (298.15 to 313.15) K with the literature value[17-18].

Apparatus and Procedure : The binary mixture is prepared by weighing appropriate amounts of pure liquids on a digital electronic balance model Shimadzuax-200 with an uncertainty of ± $1 \cdot 10^{-4}$ kg. Before each series of experiments, we calibrated the instrument at atmospheric pressure with doubly distilled water. The average uncertainty in the composition of the mixtures was estimated to be less than ±0.0001.A crystal controlled variable path ultrasonic interferometer operating at a frequency of 2 MHz was used in the ultrasonic measurements. The reported uncertainty is less than ±3% which is the highest uncertainty found from all the data points. Refractive index was measured by Abbe refractometer. Refractive index data were accurate to ±0.0001 units. The purity of chemicals used was confirmed by comparing the densities and ultrasonic speeds with those reported in the literature as shown in Table 1. The uncertainty in the density measurement was within ±0.7 $kg.m^{-3}$ (about 0.06%). The densities of the pure components and their mixtures were measured with the bi-capillary pyknometer. The liquid mixtures were prepared by mass in an air tight stopped bottle using an electronic balance model Shimadzuax-200 accurate to within ±0.1 mg. Isentropic compressibility, k_s, were calculated from the relation,

$$k_s = u^{-2}\rho^{-1} \qquad (1)$$

where ρ is the density and u is the ultrasonic velocity.

Results and Discussion

The experimental density, speed of sound, and refractive index values for binary systems of 1-butyl-3-methylimidazolium tetrafluoroborate with 1-pentanol are reported at T = (298.15 to 313.15) K and atmospheric pressure are listed in Table 2. The excess volume, V^E and excess isentropic compressibility values k_s^E were calculated from the relation as :

$$V^E = \sum_{i=1}^{n} \frac{x_I M_I}{\rho} - \sum_{i=1}^{n} \frac{x_I M_I}{\rho} \text{ and } k_s^E = k_s - k_s^{idl} \qquad (2)$$

Table 1 – Comparison of experimental density (ρ_{exp}), Refractive index (n_{exp}) and speed of sound (u_{exp}) of pure components with literature (lit) values at temperatures from T = (298.15 to 313.15) K.

Components	T/K	ρ/kg·m^{-3}		n		u/m·sec^{-1}	
		ρ_{exp}	ρ_{lit}	n_{exp}	n_{lit}	u_{exp}	u_{lit}
1-butyl-3-methylimidazoliu mtetrafluoroborate	298.15	1198.78	1200.57b	1.42058	1.4197e	1565.09	1565.1
	303.15	1195.18	1196.98	1.41913	1.4181	1553.15	1552.6
	308.15	1191.60	1194.2	1.41764	1.4166	1541.35	1540.3
	313.15	1188.04	1189.86	1.41621	1.4155	1529.69	1528.3
1-pentanol	298.15	811.00	81099	1.408	1.40784	1276	1275.4
	303.15	807	80711	1.407	1.4065	1259	1262
	308.15	803	8036	1.406	1.4047	1242	1245
	313.15	800	7999	1.404	1.40178	1226	1228

where $$k_s^{idl} = k_s x_1 + k_s x_2 \quad (3)$$

and volume fractions, ∅ were calculated from the relation;

$$\varnothing = \frac{x_i V_I}{\left(\sum_{i=1}^{n} x_i V_i\right)} \quad (4)$$

The dependency of V^E on composition is shown in Fig. 1 where all V^E values are negative for the systems under study and this is due to the interstitial accommodation of ILs into alkanols structure[5]. The negative V^E trend reflects the formation of hydrogen bonded hetero associations and the dissociation of alkanol structure as the chain length increases. This is conformed from the previously reported studies[2,3,5]. In addition as expected, V^E becomes less negative as the temperature increases for ILs with 1-propanol. The excess isentropic compressibility values k_s^E were calculated from relations by Benson *et al.*[20] where k_s^{id} is the isentropic compressibility of the ideal solution, k_s is the isentropic compressibility and it is calculated using the Laplace-Newton $V=1/u^2\rho$ where the relation is judged to be valid and therefore the speed of sound may be regarded as a thermodynamic quantity. The excess isentropic compressibility are negative for the system under study and exhibited a similar trend as the excess volume (see Fig. 2) while k^E becomes more

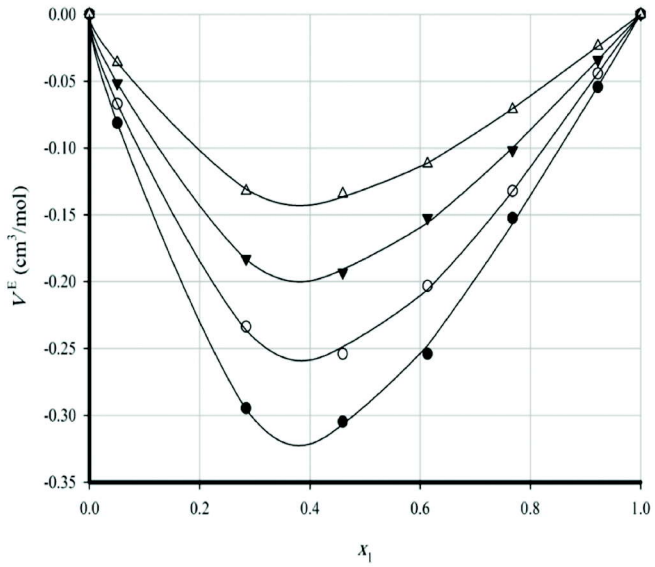

Fig. 1. Excess molar volumes, V^E, as a function of x_1 for {x [Bmim][BF4] + (1 – x) 1-pentanol} binary mixtures, at T=298K(•),303K(o),308K(▼) and 313K(Δ).

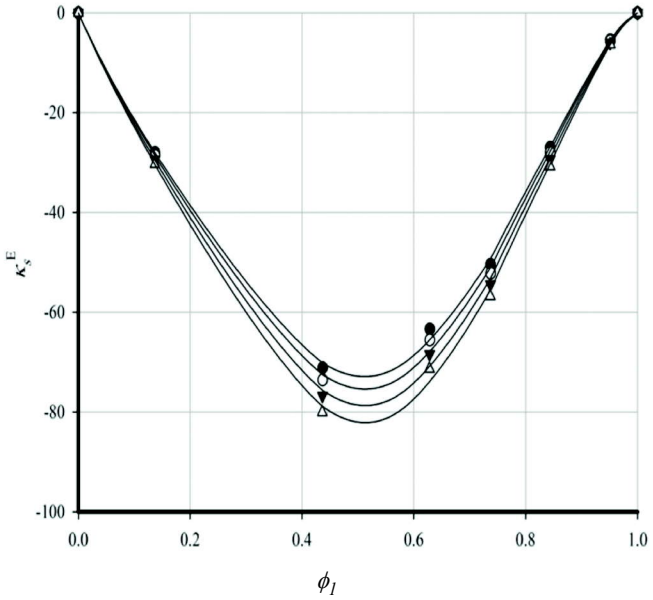

Fig. 2. Excess is entropic compressibility ∅, k_s^E, as a function of □$_1$ for {x [Bmim][BF4] + (1 – x) 1-pentanol} binary mixtures, at T=298K(•), 303K(o), 308K(▼), 313K(Δ).

negative as the temperature increases as shown in Table 2. which suggest the dominance of interstitial of accommodation of the components effect over the dissociation effect. The calculated excess properties were fitted to the Redlich-Kister (R-K) polynomial equation, Schaaff's Collision Factor Theory (CFT), Jacobson's Free Length Theory (FLT) and Nomoto's relation (NR)[9-13] were used to predict the speed of sound *(um)* for 1-butyl-3-methylimidazolium Tetrabuoroborat + 1-pentanol binary systems. The critical temperatures for the pure ILs were predicted using available data[20] since they are needed for CFT,

$$u = u_\infty \sum_{i=1}^{n} \frac{(x_i s_i)\left(\sum_{i=1}^{n} x_i B_i\right)}{V} \quad (5)$$

where u_∞ = 1600 m·s^{-1}, S_i and B_i are the space filling factor and the actual volume of the molecule per mole of pure component i in the mixture. Jacobson's Free Length Theory (FLT) can be expressed as;

$$u = \frac{K}{L_f \rho^{1/2}} \quad (6)$$

where K is the Jacobson's constant and $L_{f,m}$ is the intermolecular free length of the binary mixture and Nomoto's relation as;

$$u = \frac{K}{L_f \rho^{1/2}} \quad (7)$$

Table 2 – Experimental density (ρ_{exp}), Refractive index (n_{exp}) and speed of sound (u_{exp}) and values obtained from theoretical models (u_{Sch}, u_{Nom}, u_{Jacob} and $n_{L\text{-}L}$, $n_{D\text{-}G}$, n_{Eykman}) and isentropic compressibility (k_s) of binary liquid mixtures of 1-butyl-3- methylimidazolium tetrafluoroborate + 1-pentanol T = (298.15 to 313.15) K.

x_1	ρ_{exp} /kg·m^{-3}	n_{exp}	u_{exp}/ m·sec^{-1}	u_{Sch} /m·sec^{-}	u_{Nom} /m·sec^{-}	u_{Jacob} /m·sec^{-}	$n_{L\text{-}L}$	$n_{D\text{-}G}$	n_{Eykman}	k_s TPa^{-1}
					298.15K					
0.1045	889.12	1.4083	1287.2	1307.6	1267.2	1297.1	1.4080	1.4074	1.4087	395.47
0.2036	903.24	1.4093	1312.5	1332.2	1291.2	1304.1	1.4089	1.4082	1.4093	382.74
0.3044	951.23	1.4117	1350.2	1370.2	1331.4	1321.5	1.4113	1.4093	1.4099	372.48
0.4062	978.12	1.4127	1386.2	1401.5	1361.5	1341.2	1.4126	1.4099	1.4113	364.36
0.4946	1004.5	1.4143	1420.5	1440.2	1401.2	1358.5	1.4141	1.4121	1.4127	358.83
0.6071	1021.34	1.4151	1425.2	1461.2	1411.4	1401.2	1.4149	1.4132	1.4139	353.01
0.6973	1056.15	1.4163	1465.7	1467.5	1481.2	1445.5	1.4151	1.4136	1.4146	349.19
0.7830	1098.23	1.4189	1501.2	1488.8	1500.1	1496.2	1.4182	1.4156	1.4171	345.71
0.9106	1102.13	1.4202	1557.2	1525.4	1537.5	1522.1	1.4191	1.4172	1.4183	342.15
					303.15K					
0.1045	882.12	1.4081	1296.1	1301.2	1271.5	1290.2	1.4076	1.4074	1.4084	406.17
0.2036	893.12	1.4089	1333.4	1357.4	1297.1	1330.3	1.4083	1.4079	1.4088	392.47
0.3044	947.12	1.4111	1371.2	1381.2	1335.4	1362.3	1.4094	1.4083	1.4089	381.43
0.4062	974.13	1.4122	1400.6	1421.5	1389.7	1381.5	1.4099	1.4091	1.4107	372.67
0.4946	1000.50	1.4131	1406.5	1431.2	1400.2	1396.7	1.4111	1.4101	1.4113	366.80
0.6071	1018.60	1.4146	1437.2	1451.4	1411.5	1407.5	1.4136	1.4117	1.4123	360.47
0.6973	1051.04	1.4158	1472.5	1492.5	1461.3	1467.9	1.4148	1.4132	1.4137	356.20
0.7830	1093.15	1.4173	1501.2	1521.8	1489.3	1491.2	1.4167	1.4146	1.4172	352.62
0.9106	1098.21	1.4182	1536.3	1539.3	1517.8	1527.7	1.4178	1.4163	1.4177	348.60
					308.15K					
0.1045	872.20	1.4078	1270.2	1296.5	1251.4	1281.3	1.4074	1.4073	1.4082	417.36
0.2036	890.12	1.4086	1306.4	1322.4	1283.2	1336.4	1.4089	1.4082	1.4088	402.64
0.3044	936.04	1.4096	1341.2	1366.5	1317.5	1342.2	1.4091	1.4099	1.4097	390.76
0.4062	971.02	1.4111	1370.2	1390.2	1347.4	1367.5	1.4078	1.4107	1.4120	381.33
0.4946	997.30	1.4118	1391.6	1413.7	1368.2	1376.4	1.4112	1.4111	1.4109	374.84
0.6071	1011.41	1.4131	1421.6	1441.5	1392.2	1393.2	1.4123	1.4129	1.4121	368.10
0.6973	1034.12	1.4137	1452.8	1468.5	1411.3	1417.3	1.4129	1.4130	1.4133	363.45
0.7830	1046.17	1.4140	1489.2	1489.2	1427.5	1421.2	1.4138	1.4131	1.4144	359.34
0.9106	1088.04	1.4162	1521.2	1521.2	1459.4	1489.4	1.4154	1.4152	1.4172	355.04
					313.15K					
0.1045	861.12	1.4074	1276.1	1276.1	1236.4	1276.2	1.4074	1.4070	1.4080	4 28.90
0.2036	889.16	1.4082	1310.2	1310.2	1270.2	1286.4	1.4079	1.4076	1.4088	413.10
0.3044	932.12	1.4091	1347.5	1347.5	1301.4	1301.2	1.4092	1.4081	1.4093	400.33
0.4062	969.13	1.4098	1372.3	1372.3	1327.2	1333.4	1.4096	1.4099	1.4112	390.18
0.4946	994.02	1.4101	1394.2	1394.2	1347.5	1351.5	1.4101	1.4107	1.4117	383.16
0.6071	995.14	1.4111	1420.4	1420.4	1381.9	1389.2	1.4117	1.4123	1.4123	375.88
0.6973	1006.12	1.4123	1451.4	1451.4	1411.2	1411.3	1.4117	1.4134	1.4136	370.85
0.7830	1036.11	1.4132	1496.5	1496.5	1449.5	1437.2	1.4130	1.4133	1.4141	366.50
0.9106	1083.12	1.4141	1530.2	1530.2	1489.3	1491.4	1.4142	1.4149	1.4162	361.70

In addition, Lorentz-Lorenz (L-L), Dale-Gladstone (D-G) and Eykman (Eyk) mixing rules[14-16] were used to predict refractive indices for studied system. They are given as;

$$\frac{n^2-1}{n^2+2}=\sum_{i=1}^{n}\varnothing\left[\frac{n^2-1}{n^2+2}\right]$$
$$n-1=\sum_{i=1}^{n}\left[\varnothing_i\left(n-1\right)\right] \quad (8)$$
$$\frac{n^2-1}{n^2+0.4}=\sum_{i=1}^{n}\varnothing_i\left[\frac{n^2-1}{n^2+0.4}\right]$$

The comparison shows that Nomoto's relation for predicting speed of sound is the be stamong the relations used in the case of 1-Butyl-3- methylimidazolium Tetrafluoroborate + 1-Pentanol while both Nomoto's and Schaaff's Collision Factor Theory are also comparable. As for the refractive index mixing rules, all rules used showed good agreement with the experimental data for the system under study.

Conclusions

Density, speed of sound and refractive index and their excess or deviation properties of ILs with 1-pentanol binary mixtures have been reported at different temperatures and atmospheric pressure. Although ILs show stronger hydrogen bonding with 1-pentanol than conventional solvents. Prediction of the speed of sound can be obtained using Nomoto's relation and Schaaff's Collision Factor Theory while refractive index can be predicted using Lorentz-Lorenz, Dale-Gladstone and Eykman mixing rules for systems containing ionic liquids. In addition, The calculations showed a systematic dependence of excess and deviation properties on the chain length and on temperature for all investigated mixtures.

Acknowledgement

The authors are very thankful to the Department of Chemistry for their cooperation and help.

References

1 **Shekaari H.** and **Sedighehnaz S.M.,** Volumetric properties of ionic liquid 1,3-dimethyl imidazolium methyl sulfate + molecular solvents at T=(298.15-328.15) K, *Fluid Phase Equilib*. **291** (2010) 201-207.

2 **Wang J-Y., Zhao F-Y., Liu Y.M., Wang X-L.** and **Hu Y-Q.,** Thermo physical properties of pure 1-ethyl-3-methylimidazolium methyl sulphate and its binary mixtures with alcohols, *Fluid Phase Equilib*. **305** (2011) 114-120.

3 **Requejo P.F., Gonzalez E.J., Macedo E.A.** and **Dominguez A.J.,** Effect of the temperature on the physical properties of the pure ionic liquid 1-ethyl-3-methyl-imidazolium methyl sulfate and characterization of its binary mixtures with alcohols, *Chem. Thermodyn*. **74** (2014) 193-200.

4 **Pereiro A.B.** and **Rodiguez A.,** Thermodynamic properties of ionic liquids in organic solvents from (293.15 to 303.15) K, *J. Chem. Eng. Data* **52** (2007) 600-608.

5 **Domanska U., Pobudkowska A.** and **Wisniewska A.,** Solubility and excess molar properties of 1,3-dimethylimidazolium methyl sulfate, or 1-butyl-3-methylimidazolium methyl sulfate, or 1-butyl-3-methylimidazolium octylsulfate ionic liquids with n-alkanes and alcohols: analysis in terms of the PFP and FBT models1, *J. Solution Chem*. **35** (2006) 311- 334.

6 **Shukla R.K., Gangwar V.S.** and **Singh S.K.,** Effect of molecular structure of lubricating oil on sound velocity and bulk modulus, *J. Pure Appl. Ultrason,* **40** (4) (2018) 111-115.

7 **Shukla Rajeev Kumar., Gangwar V.S.** and **Pundhir Vivek Kumar.,** Density and speed of sound of binary liquid systems in temperature range 288.15 to 318.15 K, *J. Pure Appl. Ultrason,* **39** (2017) 18-22.

8 **Shukla R.K., Gupta G.K., Pramanik S.K., Sharma A.K.** and **Singh B.,** Comparative study of speed of sound and isentropic compressibility of chloroben-zene + benzene binary mixture from various models at temperature range 298.15 to 313.15 K, *J. Pure Appl. Ultrason,* **35** (2013) 80-86.

9 **Redlich O.** and **Kister A.T.,** Algebraic representation of thermodynamic properties and the classification of solutions, *Ind. Eng. Chem*. **40** (1948) 345-348.

10 **Schaffs W.,** Molecular Acoustics/Molekularakustik Springer-Verlag, Berlin 1963, (Chapters. XI and XII).

11 **Jacobson B.,** Intermolecular free length in the liquid state. Adiabatic and isothermal compressibilities, *Acta. Chem. Scand*. **8** (1952) 1485-1498.

12 **Jacobson B.,** Ultrasonic velocity in liquids and liquid mixtures, *J. Chem. Phys*. **20** (1952) 927-928.

13 **Nomoto O.,** Empirical formula for sound velocity in liquid mixtures, *J. Phys. Soc. Jpn*. **13** (1958) 1528-1532.

14 **Lorentz L.** and **Lorenz, L.V.,** Ueber die Refraktion Konstante, *Wied. Ann*. **11** (1880) 70-75.

15 **Gladstone J.H.** and **Dale T.P.,** Researches on the refraction and dispersion and sensitiveness of liquid, *Philos. Trans*. **153** (1863) 317-343.

16 **Eykman J.F.,** Reel. Trao. Recherches réfracto métriques (suite), *Chim Pays-Bas*. **14** (1895) 185-188.

17 **Timmermans J.,** Physico- chemical constants of pure organic compounds, 8th Ed., *Elsevier Pub. Corp. Inc., New York* (1950).

18 **Riddick J.A., Bunger W.S.** and **Sakano T.,** organic solvents, physical properties and methods of purification, 4th ed, *Johnwiley and Sons Press., New York* (1986).

19 **Letcher T.M., Domanska U.** and **Mwenesongole E.,** The excess molar volumes and enthalpies of (N-methyl-2-pyrrolidinone + an alcohol) at T = 298.15 K and the application of the ERAS theory, *Fluid Phase Equilib*. **149** (1998) 323- 337.

20 **Benson G.C.** and **Kiyohara O.,** Evaluation of excess isentropic compressibilities and isochoric heat capacities, *J. Chem. Thermodyn*. **11** (1979) 1061-1064.

21 **Al Tuwaim M.S., Alkhaldi K.H.A.E., Al-Jimaz A.S.** and **Mohammad A.A.,** Temperature dependence of physicochemical properties of imidazolium-, pyroldinium- and phosphonium-based ionic liquids, *J. Chem. Eng. Data*. **59** (2014) 1955-1963.

J. Pure Appl. Ultrason. 42 (2020) pp. 78-80

Short Communications

Elastic and ultrasonic properties of cadmium oxide

Jyoti Bala[1], Vyoma Bhalla[2,*], Devraj Singh[3], C.P. Yadav[4] and D.K. Pandey[4]

[1]University School of Information & Communication Technology,
Guru Gobind Singh Indraprastha University, New Delhi-110 078, India
[2]Amity School of Engineering & Technology Delhi, A.U.U.P. Premises, Noida-201 313, India
[3]Department of Physics, Prof. Rajendra Singh (Rajju Bhaiya) Institute of Physical Sciences for Study and Research,
Veer Bahadur Singh Purvanchal University, Jaunpur-222 003, India
[4]Department of Physics, P.P.N. (P.G.) College, Kanpur-208 001, India
*E-mail: bhallavyoma@gmail.com

The attenuation of ultrasonic waves has been estimated in rocksalt type (B1) and CsCl type (B2) structures of CdO at room temperature along <100>, <110> and <111> directions. First of all, the higher order elastic constants have been computed using Born model with Mori and Hiki approach. Then, the second order elastic constants (SOECs) were applied to compute the mechanical constants such as shear modulus, Young's modulus, bulk modulus, tetragonal modulus, Poisson's ratio, Pugh's indicator for finding performance of CdO. Numerous physical quantities, such as ultrasonic velocity, Debye temperature, thermal conductivity, ultrasonic Gruneisen parameter and acoustic coupling constants have been determined for the chosen material. Finally, the attenuation of ultrasonic waves has been compared in B1 and B2 phases of CdO and discussed in correlation with available findings.

Keywords: Cadmium oxide, elastic constants, thermal properties, ultrasonic properties.

Introduction

Over the past few years metal oxides semiconductors have received enormous attention due to their interesting electrical and optical properties in several technologically challenging areas. One of the important semiconductor material is Cadmium Oxide (CdO). It is the transparent conductive oxides (TCOS) and are of high interest from industrial applications such as liquid crystal display (LCD), photoelectric devices, gas sensors, IR detectors, etc. It normally crystallizes into rock-salt structure (NaCl) under pressure[1-4]. Sahoo *et al.*[5] carried out Ab initio calculations on structural, elastic and dynamic stability of CdO at high pressures and concluded the transformation of CdO from B1 to B2 phase under hydrostatic pressure of ~87 GPa. Bhardwaj[6] studied the structural and thermophysical properties of cadmium oxide using the Three-Body Potential (TBP) model.Jentys *et. al.*[7] studied the structural properties of CdO and CdS clusters in zeolite *Y*. The structural properties of CdO in the rock-salt (sodium chloride), cesium chloride *etc* was studied using first-principles total energy calculations by Moreno *et. al.*[8]. Dou *et. al.*[9] performed the experimental and theoretical investigation of the electronic structure of CdO using periodic Hartree-Fock and density functional methods. Piper *et. al.*[10] studied the electronic structure of single-crystal rocksalt CdO by soft x-ray spectroscopies and ab initio calculations.

In the present study, a computational approach has been followed for the investigation of ultrasonic attenuation in order to study the inherent properties of CdO. The Coulomb and Born-Mayer potentials model have been used to determine the elastic, mechanical and thermo-physical properties at room temperature. The van der Waals' forces of interaction have been neglected. To the best of our knowledge, no calculation has been done on the temperature dependent study of CdO using this model.

Theory

The temperature dependent elastic, mechanical and ultrasonic properties at room temperature have been

studied using simple Coulomb and Born-Mayer interionic potential models[11-12].

Elastic and Mechanical Properties : The evaluation of second- and third-order elastic constants (SOECs and TOECs) have beeb done using Mori and Hikki approach[13].

The elastic constants computed helps in the evaluation of mechanical properties such as bulk modulus *(B)*, Young's modulus *(Y),* shear modulus *(S)*, Poisson's ratio *(σ),* Anisotropy *(A) etc.* using the approach followed in our previous work[11,12].

Ultrasonic Properties : The relation used for finding the ultrasonic velocities for waves propagating along <100>direction for B1- and B2- type structured CdO is given in our previous work[12,14].

The ultrasonic attenuation due to phonon-phonon interaction (Akhieser loss) for longitudinal and shear modes is given by Mason[11].

Results and Discussion

The SOECs and TOECs for B1and B2 structures of CdO are computed at room temperature using the nearest neighbour distance (r_0) as 1.927Å and hardness parameter (b) as 0.123Å. The results obtained have been listed in Table 1.

Table 1 – Second and third elastic constants [in $\times 10^{11}$N/m^2] for CdO at room temperature.

CdO → SOEC/TOEC ↓	B1	B2
C_{11}	10.64	13.66
C_{12}	2.87	2.40
C_{44}	3.299	4.17
C_{111}	-160.22	-97.42
C_{112}	-11.87	-51.87
C_{123}	3.185	-59.83
C_{144}	5.459	-20.98
C_{166}	-13.44	-20.74
C_{456}	5.355	-49.67

From Table 1, the elastic constant C_{11} represents elasticity in length and is found more in B2-CdO. A longitudinal strain at room temperature produces a change in C_{11}. The elastic constants C_{12} and C_{44} are related to the elasticity in shape, which is a shear constant. A transverse strain with temperature causes a change in shape without a change in volume. Therefore, from the values of C_{12} and C_{44} in B1 and B2-CdO these are less sensitive to temperature as compared to C_{11}.

Elastic modulus *B, Y, G, σ, λ, μ , B/G* and *A* are also calculated at room temperature using evaluated SOECs and are presented in Table 2. From Table 1 the value of $C_{44}>0$ thus, the CdO is stable at room temperature according to Born stability criterion[11]. The elastic constants helps in determining the response of the crystal to external forces. They play major role in determining the strength of the material. The single crystal shear moduli for the {100} plane along the [010] direction and for the {110} plane along the [110] direction are simply given by $G_{\{100\}} = C_{44}$ and $G_{\{110\}} = (C_{11}-C_{12})/2$, respectively. It is found that the shear moduli $G_{\{100\}}$ are always lower than $G_{\{110\}}$. The obtained *v* values are less than the lower limit value of 0.25 which indicate that the interatomic forces in the B1 and B2-CdO are non-central forces. *B/G* for the chosen materials must be between 1.56 and 1.59 to be brittle in nature and thus, B1-CdO is more brittle from Table 2.

From Table 3, it is observed that the Debye average velocity *(V_D)* and Debye temperature *(T_D)* is highest for B2-CdO. The specific heat per unit volume *(CV)* and crystal energy density (E_0) have been computed from θ_D/T tables of AIP Hand book[11]. The values for C_V in 10^7J m^{-3} K^{-1} is equal to 1.58 and 0.67 for B1 and B2 CdO respectively. The value of E_0 is 3.43 × 10^9 J m^{-3} for B1-CdO and 1.34 x 10^9 J m^{-3} for B2-CdO. The acoustic coupling constants D_L and D_S (for longitudinal and shear waves) which assess the ability of thermal phonons to absorb energy from sound wave have been measured along <100>directions and is listed in Table 3. The total ultrasonic attenuation is higher for B1-CdO and the thermoelastic losses are more as compared to the values of B2-CdO in Table 3.

Table 2 – Mechanical properties of CdO at 300K.

CdO	B(GPa)	Y(GPa)	G(GPa)	λ(GPa)	H(GPa)	C_p(GPa)	B/G	σ	A	P(gm/cm^3)	$G_{\{100\}}$	$G_{\{110\}}$
B1	54.6	86.9	35.2	31.17	6.23	-4.23	1.55	0.235	0.849	8.48	3.299	3.88
B2	61.5	112.4	47.0	30.1	9.55	-17.7	1.31	0.195	0.741	3.724	4.17	5.63

Table 3 – Ultrasonic velocities, thermal conductivity and D_L, D_S, α/f^2 (in 10^{-16}Nps^{2}m^{-1}) along <100> direction of CdO compounds at 300K.

CdO → Parameters ↓	B1	B2
V_L (10^3 m s^{-1})	3.54	6.06
V_S (10^3 m s^{-1})	1.97	3.34
V_D (10^3 m s^{-1})	2.196	3.728
T_D (K)	281	363
K (Wm^{-1}K^{-1})	0.917	0.549
D_L	13.99	8.95
D_S	1.054	19.63
$(\alpha/f^2)_L$	6.01	0.336
$(\alpha/f^2)_S$	1.313	2.184
$(\alpha/f^2)_{th}$	0.021	0.002
$(\alpha/f^2)_{Total}$	7.345	2.522
τ_s(10^{-14}s)	3.59	1.75

Conclusion

On the basis of above discussion following point can be drawn:

- B1-CdO is more brittle in nature as compared to B2-CdO.
- Anisotropic factor, A is found to be smaller than unity for B1 and B2 CdO. So these are completely anisotropic materials.
- Thermal conductivity and thermal relaxation time plays an important role for total at-tenuation in these materials and is higher for B1-CdO.
- The elastic, mechanical, thermal and ultrasonic properties of CdO may be used for fur-ther investigation and in the manufacturing industries.

References

1 **Quiñones-Galván J.G., Lozada-Morales R., Jiménez-Sandoval S., Camps E., Castrejón-Sánchez V.H., Campos-González E., Zapata-Torres M., Pérez-Centeno A.** and **Santana-Aranda M.A.,** Physical properties of a non-transparent cadmium oxide thick film deposited at low fluence by pulsed laser deposition. *Mater. Res. Bull.* **76** (2016) 376-383.

2 **Sagadevan S.** and **Veeralakshmi A.,** Synthesis, Structural and Dielectric Characterization of Cadmium Oxide Nanoparticles. *Int. J. Chem. Mol. Eng.* **8** (2014) 1492-1495.

3 **Yang, Y., Jin, S., Medvedeva, J.E., Ireland, J.R., Metz, A.W., Ni, J., Hersam, M.C., Freeman, A.J.** and **Marks, T.J.,** CdO as the archetypical transparent conducting oxide. Systematics of dopant ionic radius and electronic structure effects on charge transport and band structure. *J. Am. Chem. Soc.* **127** (2005) 8796-8804.

4 **Sarma, H.** and **Sarma, K.C.,** Structural characterization of cadmium oxide nanoparticles by means of X-ray line profile analysis. *J. Basic App. Eng. Res.* **2** (2015) 1773-1780.

5 **Sahoo B.D., Joshi K.D.** and **Gupta S.C.,** Ab initio calculations on structural, elastic and dynamic sta-bility of CdO at high pressures. *J. Appl. Phys.* 112 (2012) 093523.

6 **Bhardwaj P.,** Structural and thermophysical properties of cadmium oxide. *ISRN Thermodynamics*. (2012) 1-4.

7 **Jentys A., Grimes R.W., Gale J.D.** and **Catlow C.R.A.,** Structural properties of CdO and CIS clusters in Zeolite, *Y.J. Phys. Chem.* 97 (1993) 13535-13538.

8 **Moreno R.J.G.** and **Takeuchi N.,** First principles calculations of the ground-state properties and struc-tural phase transformation in CdO. *Phys. Rev. B* **66** (2002) 205205.

9 **Dou Y., Egdell R.G., Law D.S.L., Harrison N.M.** and **Searle B.G.,** An experimental and theoretical investigation of the electronic structure of CdO. *J. Phys. Condens. Matter*. **38** (1998) 8447.

10 **Piper L.F.J., DeMasi A., Smith K.E., Schleife A., Fuchs F., Bechstedt F., Zuniga-Pérez J.** and **Munoz-Sanjosé V.,** Electronic structure of single-crystal rocksaltCdO studied by soft x-ray spectroscopies and ab initio calculations. *Phys. Rev. B* **77** (2008) 125204.

11 **Bhalla V., Kumar R., Tripathy C.** and **Singh D.,** Mechanical and thermal properties of praseodymium monopnictides: an ultrasonic study. *Int. J. Mod. Phys. B* **27** (2013) 1350116.

12 **Jyoti B., Singh S.P., Gupta M., Tripathi S., Singh D.** and **Yadav R.R.,** Investigation of zirconium nanowire by elastic, thermal and ultrasonic analysis, *Z. Naturforsch*. 2020 (Article in Press), doi: 10.1515/zna-2020-0167.

13 **Mori S.** and **Hiki Y.,** Calculation of the third-and fourth-order elastic constants of alkali halide crystals. *J. Phys. Soc. Jpn.* **45** (1975) 1449-1456.

14 **Singh D.** and **Pandey D.K.,** Ultrasonic investigations in intermetallics. *Indian Acad. Sci.* **72** (2009) 389-398.

Ph.D. Thesis Summary

Study of Ultrasonic and Thermal Properties of Materials for Industrial Applications

(Ph.D. Degree Awarded to Dr. Shakti Pratap Singh under the supervision of
Prof. (Dr.) Raja Ram Yadav by University of Allahabad, Prayagraj, India in 2020)

The whole thesis is divided into two sections which comprise eight chapters. In section A, the effort has been made to develop a theoretical approach for the evaluation of second order elastic constants (SOECs) and third order elastic constants (TOECs), ultrasonic attenuation, velocity and other associated parameters in different type of crystalline materials at different physical conditions like temperature, pressure, orientation, etc. These advanced materials are very useful for many industrial applications. The section B describes experi-mental work, deals with the development nanoparticles-liquid suspensions (nanofluids) and studies of the thermal and ultrasonic properties depending upon temperature and concentration of the nanoparticles for the purpose of industrial applications.

The nature and quality of the solid can be predicted with the help of elastic and mechanical parameters of the crystal which are well associated with the ultrasonic characteristics of the same. The SOECs and TOECs can provide valuable information regarding anharmonic properties of the crystals. The pressure and temperature-dependent studies of these elastic constants may provide the dynamic thermo-mechanical characteristics of crystals and they play important roles in the designing of industrial equipment with desirable physical properties under ambient operating conditions. Chapters 3 and 4 presented our theoretical study focus on superconducting and thermoelectric materials at low and high temperature region respectively. The superconducting MgB_2 has HCP structure used in microwave devices, cryogenic machine-building, pumps, generators, next generation MRI instruments, superconducting test cables, etc.The SOECs of MgB_2 increase monotonously with increase in pressure and followed the born stability criteria for an HCP crystal so MgB_2 is mechanically stable. The electron-phonon interaction, which is influenced by electrical resistivity, is the dominating cause of ultrasonic attenuation, occurs at low temperatures in MgB_2 single crystal.

At the higher temperature, the study of ultrasonic behaviour is crucial for the information of their physical characteristics such as specific heat, energy density, and thermal relaxation time for the solid materials, Ultrasonic attenuation along with ultrasonic velocity are related to different properties of solids such as structural inhomogeneity, nonlinearity parameters, grain size, dislocation, electrical and thermal properties. The thermoelectric ZrX_2(X=S, Se) has also HCP structureused in mechanical, chemical and thermal attributes, photoelectric, electrical and thermal conductors, batteries, broadband optical modulator, fiber laser, forming Schottky junction, etc. The second-order elastic constants of both ZrX_2(X=S, Se) decreases with increase in temperature. At all the temperature the calculated values of SOECs also followed the born stability criteria for an HCP crystal so both ZrX_2(X=S, Se) has been mechanically stable all temperatures. The phonon-phonon interaction, which is influenced by thermal conductivity, is the dominating cause of ultrasonic attenuation, occurs at higher temperatures in both ZrX_2(X=S, Se). On the behalf of the other evaluated physical properties $ZrSe_2$ is better thermoelectric material in comparison to ZrS_2.

Chapters 6 and 7 presented our experimental study on CdS/PVA and Fe_2O_3/EG nanofluids and their ultrasonic and thermal conduction behaviour. In this study, synthesis, characterization and possible applications are discussed in details. These studies are done in a wide range of temperature (20-80°C) as temperature is a crucial parameter for the heat transfer applications. Further, time dependent stability is investigated in these nanofluids. CdS and Fe_2O_3 nanoparticles have been synthesized via the co-precipitation and simple sol-gel method respectively, without using any capping agent. Ultrasonic spectroscopy method (very simple, non-radiative and cost

effective method) has been used for the determination of size of the nanoparticles and their distribution in the matrix. We have determined particle size distribution of CdS and Fe_2O_3 NPs in their base fluid. The results are in good agreement with expensive TEM method.The maximum thermal conductivity enhancement ~61% at 80°C has been observed in CdS/PVA nanofluids, with very low nanoparticle loading (1.0 wt.% of CdS NPs). This enhancement is significant large, so this nanofluid has potential applications in cooling of microchips, solar collectors *etc*. The maximum thermal conductivity enhancement in Fe_2O_3/EG nanofluids is ~ 33% at 80°C with very low nanoparticle loading (1.0 wt.% of Fe_2O_3 NPs). The employed theoretical approaches for the ultrasonic attenuation and the thermal conductivity have been explained successfully the experimental observations. The measured thermal conductivity data has great importance in the thermal management of the nano-electronic and nano-optical devices in advanced heat transfer managements in many industrial applications.

Journal of Pure and Applied Ultrasonics

(INDEXED IN: Indian Citation Index, Google Scholar, i-Scholar)

INFORMATION FOR AUTHORS

1. Type of Contribution

JOURNAL OF PURE AND APPLIED ULTRASONICS welcomes contributions on all aspects of ultrasonics including ultrasonic studies in medical ultrasonics, NDT, underwater, transducers, materials & devices and any other related topic. Contributions should fall into one of the following classes.

Paper - These should be on original research work contributing to scientific developments. They should be written with a wide readership in mind and should emphasize the significance of the work.

Reviews and Articles - Includes critical reviews and survey articles.

Research and Technical notes - These should be short descriptions of new techniques, applications, instruments and components.

Letters to the editor - Letters will be published on points arising out of published articles and papers and on questions of opinion.

Miscellaneous - Miscellaneous contributions such as studies, interpretive and tutorial articles, conference reports and news items are also accepted. Recommended contribution lengths are: Papers 2000-4000 words. Reviews and Surveys 2000-5000 words; Conference Reports 500-1500 words; News Items, Research and Technical Notes up to 1000 words.

2. Manuscripts

Manuscripts should be typed on one side of the paper in double spacing with 25 mm margin on all sides of A4 size paper. A soft copy of the manuscript in MS WORD for text and MS EXCEL for illustrations and a PDF file thereof may be sent by e-mail or CD/ DVD. Colour images should be formatted as JPEG files. Figures submitted in colour would be published in colour. Colour should be avoided unless it is required in order to convey a message or serve a purpose in the image.

Title - Titles should be short and indicate the nature of the contribution.

Abstract - An abstract of 100-200 words should be provided on the title page of paper and review article. This should indicate the full scope of the contribution and include the principal conclusions.

Mathematics - Mathematical expressions should be arranged to occupy the minimum number of lines consistent with clarity e.g., $(x^2+y^2)/(x-y)^{1/2}$.

Illustration - The line illustrations along with captions should be clearly drawn with black Indian ink. Figures in Excel are preferred.

References - References should be referred to in the text by number only. The reference number should be given as superscript. The corresponding reference shall contain the following information in order; names and initials of author (s)(bold), title of the work, journal or book title (italic), volume number (bold), year of publication in brackets, page number, e.g., **Kumar S.** and **Furuhashi H.,** Anisotropic divergence controlled ultrasonic transmitter array for three dimensional range imaging, *J. Pure Appl. Ultrason.,* **38** (2016) 49-57.

Units and Abbreviations - Authors should use SI units wherever possible.

R.N. 39355/81

KappaWave ULTRASONIC FLAW DETECTOR Model K1 & K8

State-of-the art Gate movements.

Scientific calculator for UT work

Large display. Less eye strain. See everything in detail

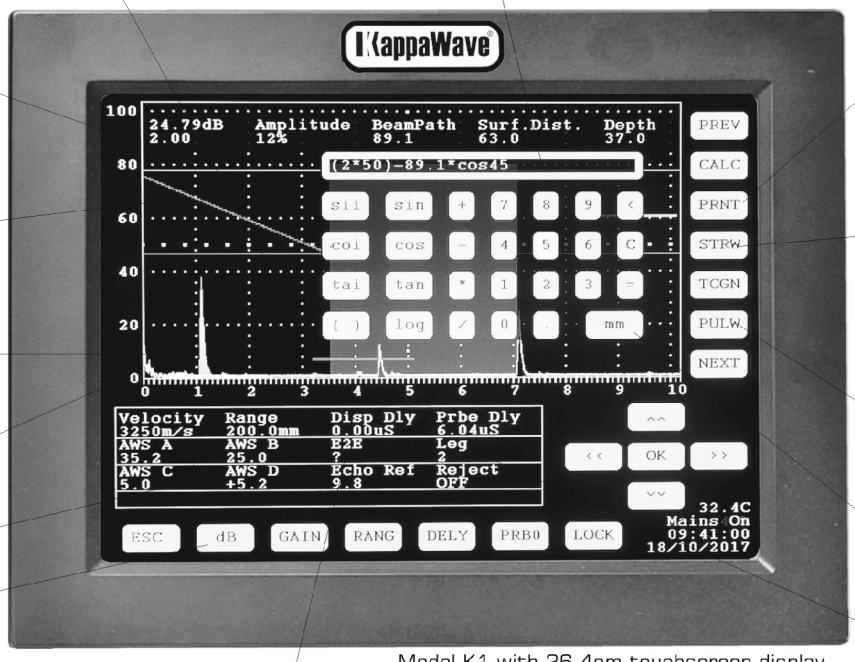

Save Test files easily
Save several thousands of files. Review any file in the instrument with relevant info

Beam plot in an Angle beam test helps you interpret signals easily

Echo store control. Ideal for transfer correction and corrosion monitoring work

Echo store

Better near surface resolution with this Pulse width control

7 Colour options

Direct mm to inch conversion

AWS D1.1 'D' value

.03, .2, 1,2,6 &12 dB increment

Leg info in an Angle beam test

Model K1 with 26.4cm touchscreen display

- 26.4 & 17.7cm Touchscreen display
- Ease of use, All touch controls
- A, B Scan & Beam plot ability
- RF Wave
- 16GB memory
- 16 hours Li-ion battery
- PC Connectivity & Reporting software
- 14 point DAC & TCG
- AWS D1.1 Weld evaluation
- Echo Store for comparisons
- Scientific calculator
- Two point Auto calibration
- VGA out
- Adjustable PRF, Damping, Pulse width and Pulse energy
- New Reject control
- Low noise
- Penetrative power
- Clear visibility in any light

Single Gate provides Echo to Echo distance

Material cross section in a B Scan

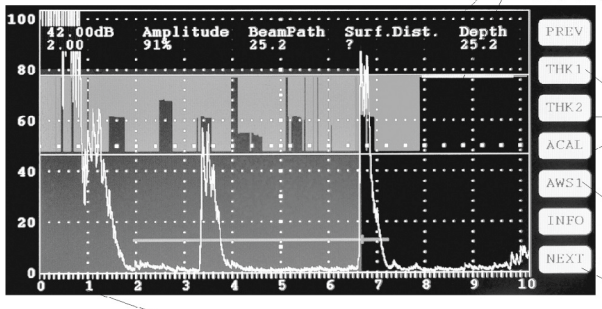

Two Point Auto Calibration

AWS D1.1 Weld evaluation

Easy to access functions

100 small divisions. 25mm to 6m Range in Steel

1.2Kg 16Hr Li-ion

Visual & Audible Alarm

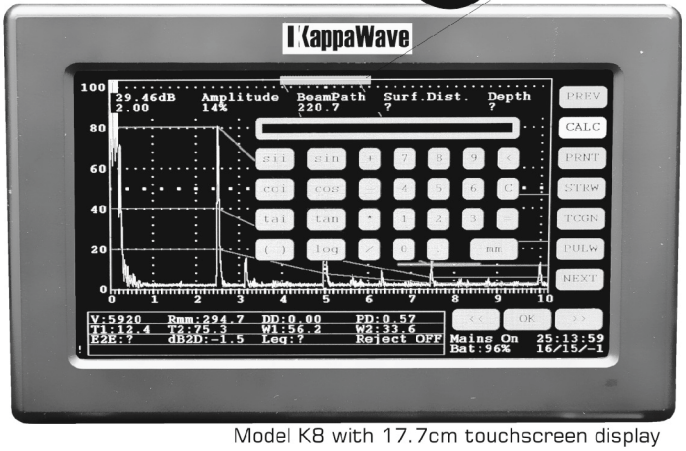

Model K8 with 17.7cm touchscreen display

Select any file to open in computer

Enter data for report

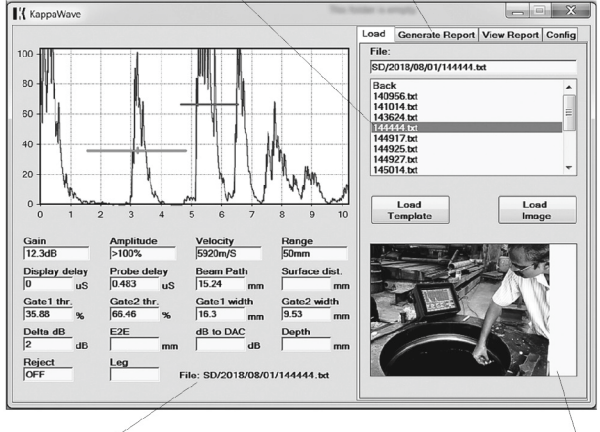

Test file info

Add photos or drawings to report

KAPPAWAVE

454, Karukancheril Buildings, Kiliroor (N) P.O.,Kottayam 686020, Kerala. Tel: Sales: 9447705887. E: sales@kappawave.com